Ship- and aircraft-based XCH$_4$ over oceans as new tool for satellite validation

Astrid Müller[1], Hiroshi Tanimoto[1], Takafumi Sugita[1], Prabir K. Patra[2,3], Shin-ichiro Nakaoka[1], Toshinobu Machida[1], Isamu Morino[1], André Butz[4,5], Kei Shiomi[6]

[1]National Institute for Environmental Studies, Tsukuba, Japan
[2]Japan Agency for Marine-Earth Science and Technology, Yokohama, Japan
[3]Research Institute for Humanity and Nature, Kyoto, Japan
[4]Institute of Environmental Physics, University of Heidelberg, Heidelberg, Germany
[5]Heidelberg Center for the Environment, University of Heidelberg, Heidelberg, Germany
[6]Earth Observation Research Center (EORC), Japan Aerospace Exploration Agency (JAXA), Tsukuba, Japan

Correspondence to: Hiroshi Tanimoto (tanimoto@nies.go.jp), Astrid Müller (mueller.astrid@nies.go.jp)

Abstract. Satellite based estimations of dry-air column-average mixing ratios of methane (XCH$_4$) contribute to a better understanding of changes in CH$_4$ emission sources and variations in its atmospheric growth rates. High accuracy of the satellite measurements is required, and therefore, extensive validation is performed, mainly against the Total Carbon Column Observing Network (TCCON). However, validation opportunities at open ocean areas outside the coastal regions are sparse. We propose a new approach to assess the accuracy of satellite derived XCH$_4$ trends and variations. We combine various ship and aircraft observations with the help of atmospheric chemistry models, mainly used for the stratospheric column, to derive observation-based XCH$_4$ (obs. XCH$_4$). Based on our previously developed approach for the application to XCO$_2$, we investigated 3 different advancements from a simple to more elaborate approaches (approach 1, 2, and 3) to account for the higher tropospheric and stratospheric variability of CH$_4$ as compared to CO$_2$. Between 2014–2018, at 20–40° N of the western Pacific, we discuss the uncertainties of the approaches and the derived obs. XCH$_4$ within 10° by 20° latitude–longitude boxes. Uncertainties were 22 ppb for approach 1, ~~and~~20 ~~17~~ ppb for approach 2, and 16 ppb for approach 3. We analysed the consistency with the nearest TCCON stations and found agreement of approach 3 with Saga of 1 ± 12 ppb, and −1 ± 11 ppb with Tsukuba for the northern and southern latitude box, respectively. Furthermore, we discuss the impact of the modelled stratospheric column on the derived obs. XCH$_4$ by applying 3 different models in our approaches. Depending on the models, the difference can be more than 12 ppb (0.~~5~~6 %), showing the importance for the appropriate choice. We show that our obs. XCH$_4$ dataset accurately captures seasonal variations of CH$_4$ over the ocean. Using different retrievals of the Greenhouse gases Observing Satellite (GOSAT) from the National Institute for Environmental Studies (NIES), the RemoTeC full-physics retrieval operated at the Netherlands Institute for Space Research (SRON), and the full-physics retrieval of the University of Leicester (UoL-OCFP), we demonstrate the applicability of the dataset for satellite evaluation. The comparison with results of approach 3 revealed that NIES showed a difference of −0.04 ± 13 ppb and strong scatter at 20–30° N, while RemoTeC and OCFP have rather systematic negative bias of −12.1 ± 8.1 ppb and −10.3 ± 9.6 ppb. Our new

approach to derive XCH4 reference datasets over the ocean can contribute to the validation of existing and upcoming satellite missions in future.

1 Introduction

Methane (CH4) is ~~one of~~ the second most important anthropogenic greenhouse gas~~es~~ (GHG) in the atmosphere after ~~besides~~ carbon dioxide (CO2). Since the pre-industrial reference year of 1750, the annual average surface dry-air mole fraction of CH4 has more than doubled from 729 parts per billion (ppb) to 1866 ppb in 2019 (Canadell et al., 2021). The global warming potential (GWP) over a 100-year period is 28–36 times that of CO2 (Forster et al., 2007). It is estimated that CH4 contributed with 0.5°C to the recent global warming between 2010–2019 relative to 1850–1900 (IPCC, 2021). Compared to CO2, the global atmospheric lifetime of 9.1 years is short (Szopa et al., 2021). Consequently, a reduction in CH4 emission is expected to lead to a quick decrease of global CH4 concentrations and therefore, to short-term mitigation of global warming (Saunois et al., 2020; Shindell et al., 2012).

The wide variation of the mean growth rate of CH4 in the past 3 decades and its rapid rise in the recent years are poorly understood (Canadell et al., 2021; Nisbet et al., 2019; Zhang et al., 2022). While the renewed increase of CH4 was primarily attributed to anthropogenic activities (Zhang et al., 2022), the specific increase in 2020 could be related to lower methane sinks as a consequence of the COVID-19 lockdown and higher wetland emissions (Peng et al., 2022; Stevenson et al., 2022). However, high uncertainties in the processes affecting CH4 sources and sinks remain (e.g., Dlugokencky et al., 2009; Patra et al., 2016; Saunois et al., 2020). With about 90%, the oxidation with OH radicals is the major CH4 sink. It occurs mostly in the troposphere, through which CH4 contributes to the production of tropospheric ozone (O_3) (Myhre et al., 2013; Saunois et al., 2020; Kirschke et al., 2013). A smaller part of CH4 is removed by OH oxidation in the stratosphere, where CH4 contributes to the production of stratospheric water vapor (Myhre et al., 2013; Kirschke et al., 2013). An important uncertainty factor in estimating the strength of CH4 sinks is the distribution and variability of OH radicals (Patra et al., 2016; Zhao et al., 2019).

Precise surface and aircraft CH4 in situ measurements are conducted by global networks such as the Cooperative Air Sampling Network of the National Oceanic and Atmospheric Administration Earth System Research Laboratory (NOAA ESRL) (Dlugokencky et al., 2009) and aircraft campaigns such as the HIAPER Pole-to-Pole Observations (HIPPO) campaign (Wofsy, 2011). However, the spatial and temporal coverage is sparse, and vertical coverage is mostly limited to the troposphere. Satellite observations provide global coverage of the column-averaged dry-air mixing ratios of CH4 (denoted XCH4). To obtain information on CH4 sources and sinks, satellite instruments need to be sensitive to variations at near-surface CH4 concentration (Buchwitz et al., 2017). This was given for observations by the Scanning Imaging Absorption Spectrometer for Atmospheric Cartography (SCIAMACHY) on the Environmental Satellite (ENVISAT) (Bovensmann et al., 1999; Frankenberg et al., 2005, Schneising et al., 2011, completed mission 2002–2012), the Thermal And Near infrared Sensor for carbon Observations-Fourier Transform Spectrometer (TANSO-FTS) on-board the Greenhouse gases Observing

2

Satellite (GOSAT, launched in 2009, Kuze et al., 2009; Yoshida et al., 2011), the Tropospheric Monitoring Instrument (TROPOMI) on board the Sentinel 5 Precursor satellite (launched 2017, Veefkind et al., 2012; Lorente et al., 2021), TANSO-2 on-bord GOSAT-2 (launched in 2018, Suto et al., 2021; Yoshida et al., 2023) or the scheduled GOSAT-GW mission (to be launched 2024, https://gosat-gw.nies.go.jp/en/). These instruments collect spectra of near-infrared (NIR) and shortwave-infrared (SWIR) solar radiation reflected from the Earth's surface, covering the relevant absorption bands of CO_2, CH_4 and O_2. From these spectra, XCH_4 can be derived (e.g., Yoshida et al., 2011, 2013).

Typical variations of XCH_4 that relate to sources at the surface are on the order of a few percent at most. Therefore, to be useful for estimating surface fluxes, satellite measurements of XCH_4 require high precision, and low random and systematic errors (Buchwitz et al., 2020; Meirink et al., 2006). To achieve these requirements, extensive validation of satellite XCH_4 has been performed, mainly against data of the land-based Total Carbon Column Observing Network (TCCON) (Wunch et al., 2011), which is a network of sun-viewing ground based Fourier transform infrared (FTIR) spectrometers.

70% of the Earth surface is covered by oceans. The marine atmosphere is often influenced by the outflow of continental CH_4 emissions, and it is thought that at least half of the CH_4 oxidation occurs over oceans (Travis et al., 2020). Satellite retrievals over the oceans, however, have undergone few evaluations since validation opportunities are sparse. They are mostly limited to TCCON sites on islands and the coast, or to episodic measurement campaigns like those of the HIPPO airborne campaign (Wofsy, 2011) or of individual ship deployments (Klappenbach et al., 2015; Knapp et al., 2021). Continuous reference data of open ocean areas outside the coastal regions remain scarce.

We propose a new approach to assess the accuracy of satellite derived XCH_4 trends and variations over open ocean regions by combining commercial ship and various aircraft observations with the help of atmospheric chemistry models. We are targeting an accuracy better than that required for the GOSAT and TROPOMI mission of <35 ppb (<2%) (ESA, 2017, Nakajima et al., 2010). Our This approach was successfully applied to the evaluation of satellite XCO_2 previously (Müller et al., 2021). In contrast to CO_2, CH_4 shows higher variability due to its complex interactions between sources and sinks in the troposphere, and additionally, through the stratosphere-troposphere exchange and its stratospheric sinks. To account for this variability, we present the advancement of our previously developed approach and discuss its uncertainties, challenges, and the potential for the continuous validation of satellite observations over oceans in future.

2 Observational and model data

2.1 Aircraft

As part of Japan's Comprehensive Observation Network for Trace gases by Airliner, CONTRAIL, air samples of CH_4 are collected by the Automatic air Sampling Equipment (ASE) and Manual air Sampling Equipment (MSE) about twice a month between Japan, Hawaii, and Australia since 2005. The sampling locations of the CONTRAIL data are shown in **Fig. 1**. From mid-2017, no data are collected over the western Pacific due to a change of the aircraft type. Within the next 2 years, the resumption of aircraft observations is expected. In cooperation with Japan Airlines (JAL), the ASE is installed in the cargo

compartment on Boeing 747-400 and 777-200ER aircrafts (Machida et al., 2008; Matsueda et al., 2008). Details of the ASE are described elsewhere (Machida et al., 2008; Matsueda et al., 2008). During one flight, 12 samples are collected at the cruising altitude of about 9–12 km by using the air-conditioning system of the aircraft. The trace gas concentrations were measured at the National Institute for Environmental Studies (NIES), Tsukuba, Japan. The air samples were dried by passing through a glass trap cooled to −80°C (Machida et al., 2008). The CH_4 dry-air mixing ratio of each air sample was determined against the NIES-94 CH_4 scale, which is traceable to the standard gas scale of the World Meteorological Organization (WMO) (Dlugokencky, 2005), by using a gas chromatograph equipped with a flame ionization detector (GC-FID; Agilent Technologies, HP-5890 and 7890) (Machida et al., 2008). The analytical precision for repetitive measurements is 1.7 ppb.

Measurements with the MSE are conducted when the ASE cannot be operated. Sample air is taken from the air outlet nozzle in the cockpit using a manual diaphragm pump. The sampling method is similar to that used during aircraft observations by the Japan Meteorological Agency (JMA) (Tsuboi et al., 2013; Niwa et al., 2014). Only ASE and MSE data which were obtained below the tropopause height during the cruising part of the flight at around 11 km altitude (~200 hPa) are used. We used the blended tropopause pressure (TROPPB) to define the tropopause height, which is explained in detail in **section 2.3**. Data of the lower stratosphere were only occasionally obtained and screened out.

Air samples of the mid-troposphere at about 6 km altitude (~450 hPa) were collected by a cargo aircraft C-130H between Kanagawa (35°27' N, 139°27' E) Prefecture near Tokyo and Minamitorishima (MNM) (24°17' N, 153°59' E) about 2000 km southeast of Tokyo. The observations were conducted by JMA in cooperation with the Japan Ministry of Defense about twice a month, either by direct flights or via Iwo Jima (24°47' N, 141°19'), about 1000 km south of Tokyo. Air samples from the air-conditioning system were collected and analyzed at the JMA using a cavity ring-down spectroscopy (CRDS) analyzer (Picarro Inc., Santa Clara, CA, USA, G2301) (Saito, 2022). The concentrations of CH_4 are determined by the JMA standard gases that are traceable to the WMO standard scales. The reproducibility of CH_4 concentration of different flasks has a precision of ±0.68 ppb (Tsuboi et al., 2013).

2.2 Ship

Commercial cargo Ships of Opportunity (SOOP) have been collecting air samples since 2001 between Japan and North America, since 2005 between Japan and Australia and New Zealand, and since 2007, between Japan and Southeast Asia. In this study, we used CH_4 observations by the cargo ship Trans Future 5 (TF5, Toyofuji Shipping Co., Ltd.), which sails between Japan, Australia, and New Zealand (Fig. 1). Each round trip takes about 5 weeks (Terao et al., 2011). Concentrations of CH_4 were continuously measured using CRDS analyzer (Picarro, models EnviroSense 3000i and G1202). In parallel, concentrations of CO_2 and O_3 were measured. The same instrumentation and analysis methodology was used and described in detail in Nara et al. (2014). In short, the air intake was placed at the bow on the top of the bridge at about 28 m above sea level, 163 m away from the smokestack at the stern (Terao et al., 2011). Exhaust contaminated samples were rejected when the dry-air mole fractions of CO_2 and O_3 showed an abrupt increase and decrease, respectively. The analytical

130   precision for 1-min measurements was 0.5 ppb. Calibration with three standard gases was performed for 30 min (10 min for the respective gas) once every two days. The standard gases were calibrated against the NIES-94 CH_4 scale.

In addition, atmospheric CH_4 data collected by the research vessel Ryofu Maru (RYF, operated by JMA) at the Pacific Ocean were used (Enyo and Kadono, 2021). The intake for air samples was about 8 meters above the sea surface. Air samples were dried and the mole fraction of CH_4 was determined by gas chromatography (SHIMADZU, GC-8A). After

135   2016, data were collected using off-axis integrated cavity output spectroscopy (Los Gatos Research, GGA-30r). Calibration with 3 standard gases was performed every hour, and every 12 hours after 2016.

2.3 Models

The Model for Interdisciplinary Research On Climate Earth System, version 4.0 (MIROC4) -based Atmospheric Chemistry Transport model (ACTM) has a horizontal resolution of triangular 42 truncation (T42) which corresponds to approximately

140   2.8° longitude by 2.8° latitude. Details of the MIROC4-ACTM are described in Patra et al. (2018). The MIROC4-ACTM uses 67 vertical layers between the Earth's surface and 0.0128 hPa. Hybrid vertical coordinates are used to resolve gravity wave propagation in the stratosphere, where at least 30 model layers reside. The ACTMs are nudged with the Japanese 55-year Reanalysis data (JRA-55; Kobayashi et al., 2015) for horizontal winds and temperature at Newtonian relaxation times of 1-hour and 5-hours, respectively. A high accuracy of the MIROC4-ACTM is indicated by the agreement of simulated and

145   observed "age of air", and the inter-hemispheric gradient of SF_6 (Patra et al., 2018).

The Copernicus Atmosphere Monitoring Service (CAMS), operated by the European Centre for Medium-Range Weather Forecasts (ECMWF), provides global greenhouse gas reanalysis (EGG4) data. The CAMS reanalysis dataset assimilates satellite observations of atmospheric trace gases and global emission datasets. The horizontal resolution at a spectral truncation of T255 corresponds to a 0.7° × 0.7° (longitude–latitude) grid. The vertical model resolution consists of 60 hybrid

150   sigma-pressure levels which are interpolated to 25 pressure levels between 1000 hPa and 1 hPa, with about 12 levels in the stratosphere (Inness et al., 2019). In this study, we used EGG4 CH_4 data with monthly average fields, version v20r2. Furthermore, we used the CAMS global inversion-optimized greenhouse gas fluxes and concentrations dataset (CAMSinv) v20r1 which accounts for chemical loss in the troposphere and stratosphere. The inversion-optimized dataset has a horizontal resolution of a 2° × 3° (longitude–latitude) grid, and 34 pressure levels between 1001 hPa and 0.5 hPa (Segers and Steinke,

155   2022). We choose datasets which assimilate NOAA surface observations, but not GOSAT observations to ensure that the model results in our approach are independent from the satellite we aim to validate.

Furthermore, we extracted data of the TROPPB, which is defined as a combination of a thermal tropopause- and dynamic tropopause pressure (Wilcox et al., 2012). The TROPPB data are extracted from GEOS-FP IT (Goddard Earth Observing System-Forward Processing for Instrument Teams) meteorology data using the python suite "ginput" version 1.0.6

160   (Laughner et al., 2022). At 10° × 20° latitude–longitude boxes (**section 3.1**), the TROPPB was calculated daily every 3 hours for the center and the 4 corner locations, and was then monthly averaged.

2.4 Satellite

Japan's GOSAT launched in 2009, was developed to characterize the variability of the atmospheric CO_2 and CH_4 fractions at regional scales over the globe. The TANSO-FTS instrument on board GOSAT measures the reflected sunlight in three SWIR channels: centered at 0.764 µm (Band 1), at 1.61 µm (Band 2), and at 2.06 µm (Band 3) (Kuze et al., 2009). XCH_4 is estimated by taking ratio of the total column amounts of CH_4 and the total column of dry-air which are extending from the Earth's surface to the top of the atmosphere.

The methodology to derive XCH_4 depends on the retrieval algorithm. For the NIES retrieval, profiles of the dry-air partial columns of CO_2, CH_4, O_2, and water vapor (H_2O) were simultaneously retrieved based on the maximum a posteriori (MAP) retrieval (Rodgers, 2000; Yoshida et al., 2013). The total column of dry-air is primarily derived from the surface pressure in consideration of the retrieved H_2O profile and meteorological profiles from JMA (Yoshida et al., 2011, 2013). In case of the RemoTeC full-physics retrieval, operated at the Netherlands Institute for Space Research (SRON), The European Space Agency (ESA), and at Heidelberg University, Germany, the dry-air column is calculated from ECMWF meteorological data (Butz et al., 2011). Another full-physics retrieval of the University of Leicester is based on the original Orbiting Carbon Observatory (OCO) retrieval and was modified for use with GOSAT spectra (UoL-OCFP) (Boesch and Noia, 2023). Furthermore, NIES, RemoTeC, and UoL-OCFP differ in the number of vertical layers and the aerosol parametrization which includes the number of aerosol types (Yoshida et al., 2013; Butz et al., 2011; Guerlet et al., 2013; Takagi et al., 2014; Boesch and Noia, 2023).

In this study, we selected level 2 XCH_4 data in sun-glint mode from the NIES v02.95, the RemoTeC v2.3.8 full-physics retrieval from SRON, and the UoL-OCFP v7.3 (Copernicus Climate Change Service, Climate Data Store, 2018). A comparison with the RemoTeC v2.4.0 full-physics retrieval operated at Heidelberg University is shown in **Appendix A (Fig. A~~3~~4)**. All data were bias corrected and cloud screened using the cloud flags obtained from the TANSO-Cloud and Aerosol Imager (CAI) onboard GOSAT (Yoshida et al., 2011, 2013; Butz et al., 2011). In the following we refer to data obtained by the retrieval algorithm from NIES v02.95, RemoTeC v2.3.8, and UoL-OCFP v7.3 simply as "NIES", "RemoTeC", and "OCFP", respectively. The comparison with XCH_4 data retrieved from other satellites like GOSAT 2, launched in 2018, and TROPOMI, launched end of 2017, was not possible in our study due to missing aircraft data after mid-2017 (**section 2.1**).

3 Methodology

3.1 Study region

Figure 1 shows the study region and location of CH_4 in situ data. All data obtained over land are excluded. We selected the latitude–longitude ranges g1 = 30–40° N, 130–150° E and g2 = 20–30° N, 130–150° E of the western Pacific for the years from 2014 to end of 2017 for 2 reasons. First, we want to use the same years and region where we successfully derived ship-aircraft based column-average dry-air mole fraction of CO_2, previously (Müller et al., 2021). $10° \times 20°$ latitude–longitude

boxes were chosen to obtain enough co-located data for the seasonal and interannual comparison with satellite retrievals, where g1 is expected to be stronger influenced by the emission outflow from land as compared to g2 **(Fig. 1)**. Second, the temporal and spatial coincident ship and aircraft CH_4 data are currently limited to the northern West Pacific until mid-2017 **(section 2.1)**. Within the two latitude–longitude boxes, we calculate monthly averages of the satellite and in situ observations, and model results. The average number of monthly satellite observations at g1 and g2 of NIES is 28 ± 13 (24 months) and 34 ± 24 (31 months), of RemoTeC 24 ± 16 (11 months) and 41 ± 24 (24 month), and of OCFP 8 ± 2 (6 months) and 14 ± 11 (27 months), respectively. Months with less than 5 observations are excluded. Ship observations of TF5 and RYF from south and east of Japan were combined. On average, we obtained 6 ± 4 days of ship observations each month. The number of monthly aircraft observations was 2 ± 1 for both latitude ranges. In our study, we develop the methodology for the future application with higher numbers of in situ data.
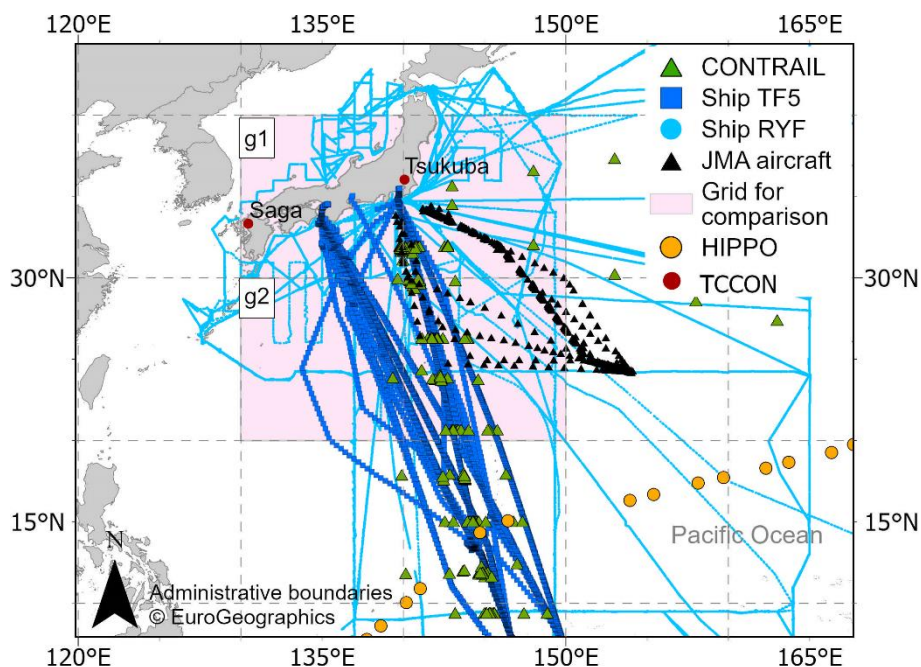

Figure 1: Location of CH_4 in situ data from aircraft (CONTRAIL: green triangles, JMA aircraft: black triangles), ship (Ship TF5: blue squares, Ship RYF: light blue circles) between 2014 and 2018. Also shown are the location of TCCON stations (red circles) and HIPPO profile flights (yellow circles). Selected regions within $10° \times 20°$ latitude–longitude boxes are shown as pink shaded areas. Administrative boundaries © EuroGeographics.

3.2 Observation-based CH_4 profile construction and XCH_4 calculation

Figure 2 illustrates the principle of how to construct ship–aircraft based CH_4 profiles from which XCH_4 is derived. Ship data are extrapolated vertically up to ~850 hPa, which represents the pressure level of the boundary layer above sea level. During boreal summer, a higher OH concentration contributes to an increased CH_4 is mainly removedal by OH oxidation at our study region (Travis et al., 2020). Including other atmospheric factors, such as atmospheric circulation pattern, models estimate the and has an instantaneous lifetime of CH_4 for July to be as short as 1 year (Fig. 14 in Patra et al., 2009, Saunois et

7

al., 2020). In the same period, the CH_4 concentration can be increased in the mid-to-upper troposphere at the western Pacific by CH_4 rich airmasses transported from South and East Asia (Umezawa et al., 2012). To constrain the tropospheric CH_4 variability, CONTRAIL aircraft data from the cruise portion of the flight at around 200 hPa, and JMA aircraft data from about 450 hPa are selected, which represents the upper and middle troposphere, respectively.
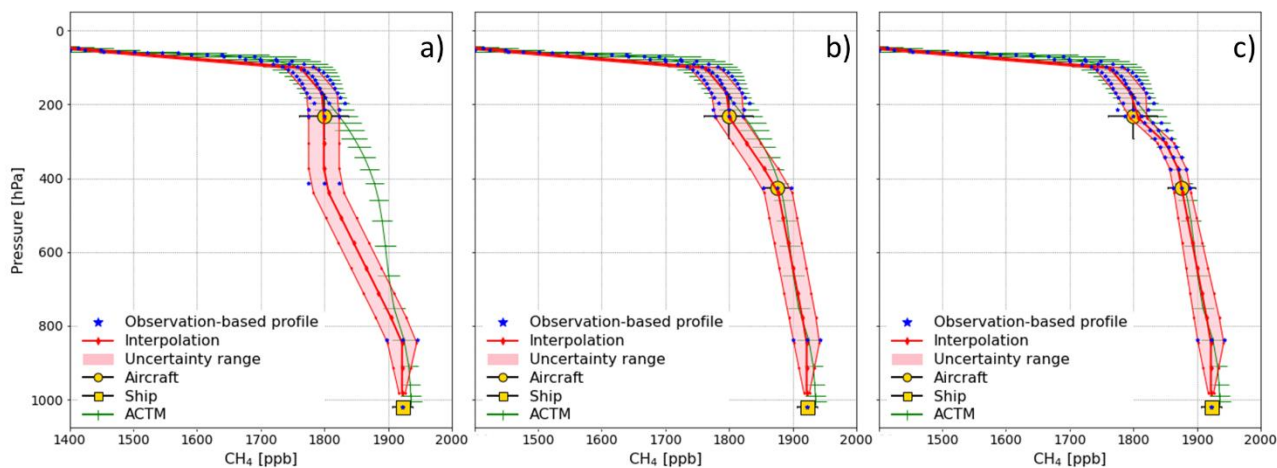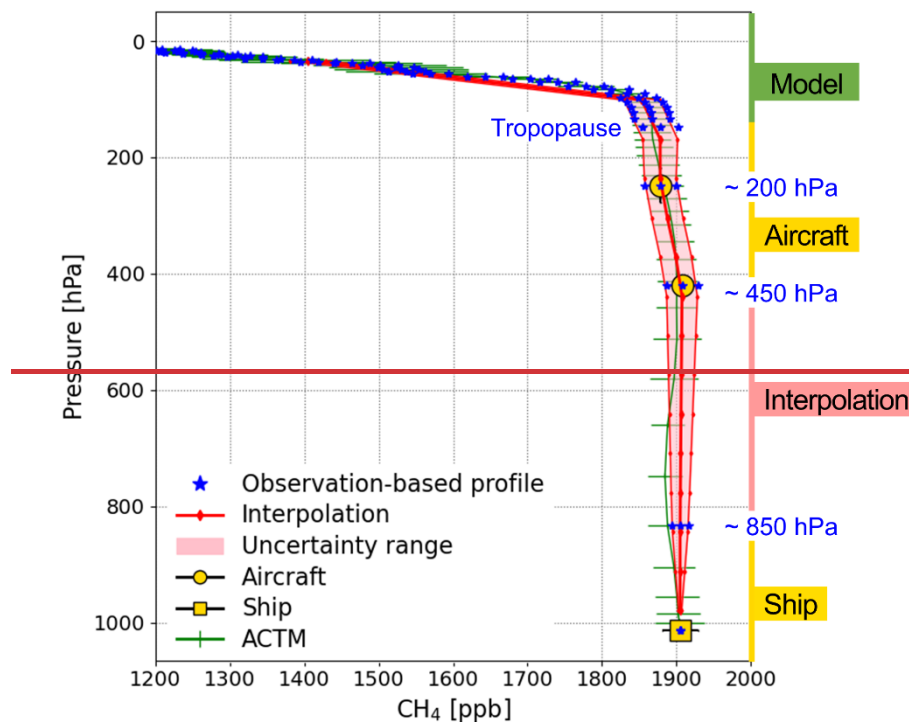
Figure 2: Construction of the observation-based CH$_4$ profile (blue) obtained by using ship and aircraft data (yellow) together with model results (green), and the interpolation onto the pressure grid of the satellite retrieval (red) for approach 1 a), approach 2 b), and approach 3 c). The example is obtained at the latitude 30–40° N, in SeptemberMarch 2015.

In the following, we test 3 approaches. Approach 1 is the adaptation of the approach of Müller et al. (2021) **(Fig. 2a)**. We extrapolate CONTRAIL data upwards to the TROPPB and downwards to the lower cruising height at 400 hPa without the

225 constraint of the JMA aircraft data. Then we linearly interpolate in both pressure and dry-air mole fraction between the extrapolated ship data, and the extrapolated aircraft data. Approach 2 is the addition of JMA aircraft data to the mid troposphere (Fig. 2b). We linearly interpolate between the extrapolated ship data, and both aircraft data (Fig. 2). In approach 3, we fill in model results between the aircraft data of JMA and CONTRAIL of approach 2 (Fig. 2c). Since CONTRAIL flies very close to the TROPPB, we do not fill model data between CONTRAIL and the TROPPB. Above the TROPPB, we use

230 model results in all three approaches. To calculate the XCH$_4$ that the satellite would have seen given our constructed CH$_4$ profile, we first interpolate these profiles onto the corresponding monthly averaged pressure grid of the satellite retrievals, then we use Eq. (15) of Connor et al. (2008):

$$X_{CH4}^m = X_{CH4}^a + \sum_j h_j \, a_{CH4,j} \, (x_m - x_a)_j \,, \tag{1}$$

where X_{CH4}^m is that XCH$_4$ which the satellite would report if it observed the constructed CH$_4$ profile x_m (as a true profile).

235 Extracted from the satellite retrievals, X_{CH4}^a is the a priori XCH$_4$, h_j the pressure weighting function, $a_{CH4,j}$ the column averaging kernel, and x_a the a priori CH$_4$ profile. In this study, we use only the pressure grid and parameters of NIES. In the following, we refer to the calculated X_{CH4}^m as "simple observation-based XCH$_4$" (simple obs. XCH$_4$), "observation-based XCH$_4$" (obs. XCH$_4$), and "model blended observation-based XCH$_4$" (blended obs. XCH$_4$) for results of approach 1, 2 and 3, respectively.

240 **3.3 Uncertainty assessment of obs. CH$_4$ profiles**

There are two uncertainty sources. The first uncertainty source arises from the limited number and spatiotemporal distribution of in situ data within the latitude-longitude boxes of each month. Therefore, the data may not always represent the monthly averaged CH$_4$ concentration within the area of interest accurately. However, in the near future, the number of in situ data will increase and the spatial distribution expands as discussed in chapter 5. The second source of Uuncertainties in

245 the obs. XCH$_4$ (simple, blended) are caused by the CH$_4$ profile construction: a) the inter- and extrapolation of the in situ data in the troposphere, b) the tropopause height, and c) the modelled stratospheric column.

3.3.1 Tropospheric uncertainty

First, to assess the uncertainty due to the inter- and extrapolation, we investigated the variability of the CH$_4$ dry-air mole fractions observed by profile flights of the HIPPO number 4 campaign (HIPPO 4) over the Pacific Ocean (Wofsy, 2011).

250 Between 14 June to 11 July 2011, 20 profiles ranging from the surface up to about 13 km were obtained near the study region (**Fig. 1**). Within each profile, the CH$_4$ dry-air mole fractions show variations between 9–62 ppb (24 ± 17 ppb, **Table 1**). The highest range was seen in the middle to upper troposphere during these summer months, consistent with observations by Umezawa et al. (2012). Based on this variation, we use 24 ppb uncertainty between the extrapolated ship data and the TROPPB for the profile construction in approach 1.

Table 1: Uncertainty assessment of the obs. CH_4 profiles at the troposphere. Top rows: average concentration range of CH_4 within each HIPPO 4 profile (mean variability ± standard deviation). Bottom rows: Root-mean-square error (RMSE) of the difference between MIROC4-ACTM (ACTM) and HIPPO 4, and MIROC4-ACTM and obs. CH_4 profile data at different altitude ranges. The last column shows the total uncertainty after Gaussian Error propagation. Uncertainties applied to approach 3 are shown in bold.

HIPPO 4 profile range [m]		Variation within profiles [ppb]	
~300–~13000		24 ± 17	

Altitude [m]	ACTM – HIPPO 4 [ppb]	ACTM – obs. CH_4 [ppb]	Total uncertainty [ppb]
0–1500	8	18	20
1500–6000	12	17	**21**
6000–11000	**13**	18	22

~~HIPPO 4 profile range [m]~~	~~Variation within profiles [ppb]~~
~~300–~13000~~	~~24 ± 17~~

~~Altitude [m]~~	~~ACTM – HIPPO4 [ppb]~~
~~0–1500~~	~~12 ± 3~~
~~1500–6000~~	~~0 ± 11~~
~~6000–11000~~	~~6 ± 15~~

Second, we assessed the uncertainty of the constructed CH_4 profiles in 3 steps with the help of the MIROC4-ACTM. In the first step, we investigate how good the MIROC4-ACTM reproduces the variation of 6 selected HIPPO profiles for similar conditions to our study region, which is influenced by the continental emission outflow (**Appendix A, Fig. A1**). Therefore, we selected 8 profiles within 2000 km of the center location of g2 near the study area (**Fig. 1**). We choose the MIROC4-ACTM to be consistent with our previous study (Müller et al., 2021). We distinguished the altitude range 0–1500 m, corresponding to the boundary layer, 1500–6000 m, corresponding to the middle troposphere between the extrapolated ship and JMA aircraft data, and 6000–11000 m, corresponding to the upper troposphere between the JMA and CONTRAIL aircraft data. As model uncertainty, we obtain tThe root-mean-square error (RMSE) of the average difference between the MIROC4-ACTM and the HIPPO profiles with were 12 ± 38 ppb, 0 ± 1112 ppb, and 6 ± 1513 ppb for the altitude ranges 0–1500 m, 1500–6000 m, and 6000–11000 m, respectively (**Table 1**). In the second step, we compare the MIROC4-ACTM with our obs. CH_4 profiles and obtain the RMSE (**Table 1**, ACTM – obs. CH_4). Because the model itself has an uncertainty as obtained in step 1, the tropospheric uncertainty of the constructed profile of each altitude range is 20 ppb, 21 ppb, and 22 ppb using Gaussian Error propagation (**Table 1**, Total uncertainty). As a result, Considering the maximum possible difference, we added 1121 ppb uncertainty between the extrapolated ship and JMA data in approach 2 and 3, and 2221 ppb and 13 ppb between the JMA data and up to the TROPPB in approach 2 and 3, respectively.

3.3.2 Tropopause uncertainty

The variation of the monthly averaged TROPPB (**section 2.3**) at 30–40° N was more than twice that at 20–30° N with an average standard deviation of 68 ± 22 hPa and 23 ± 9 hPa, respectively (**Table 2**). The maximum difference of 90 hPa (68 + 22 hPa) and 32 hPa (23 + 9 hPa) at the level of the TROPPB corresponds to an altitude difference of 3 to 4 km, and 1 to 2 km, respectively. To test the impact of the TROPPB on the derived XCH_4, we first calculated the simple obs. XCH_4. Second, we calculated the simple obs. XCH_4 with TROPPB ± 90 hPa at 30–40° N and TROPPB ± 32 hPa at 20-30° N, based on the monthly averaged variability of the TROPPB. Then, we compared the latter two results with the original simple obs. XCH_4. The average difference in the resulting XCH_4 at 30–40° N and 20–30° N for the reduced TROPPB (−90 hPa, −32 hPa) was −4 ± 3 ppb and −1 ± 1 ppb, respectively. If the TROPPB was increased (+90 hPa, +32 hPa), the difference was small as 1 ± 2 ppb and 0.1 ± 0.2 ppb (**Table 2**). Because model results are used above the TROPPB, a "too high" TROPPB (= too low altitude), can be compensated by the model. In total, the TROPPB causes an uncertainty of less than 0.4% on the calculated XCH_4.

Table 2: Uncertainty assessment of the obs. CH_4 profile. **a)** at the blended tropopause pressure (TROPPB) by calculating the difference "simple obs. XCH_4 − simple obs. XCH_4 + reduced/ increased TROPPB ($XCH_{4\,(\pm TROPPB\ var)}$)" (mean difference ± standard deviation of differences). TROPPB var = monthly average variability of TROPPB (mean standard deviation of the monthly averages ± standard deviation). **b)** at the stratospheric column by calculating the difference "simple obs. XCH_4 – simple obs. XCH_4 with extrapolated aircraft data up to 0.0128 hPa ($XCH_{4(no\_str)}$)", and the differences between the modelled stratosphere of MIROC4-ACTM (ACTM), CAMS, and CAMSinv (mean difference ± standard deviation of differences).

a) Tropopause pressure (TROPPB)	Latitude 30–40°N	Latitude 20–30°N
monthly average TROPPB variation (TROPPB var) [hPa]	68 ± 22	23 ± 9
simple obs. XCH_4 − $XCH_{4\,(−TROPPB\ var)}$ [ppb]	−4 ± 3	−1 ± 1
simple obs. XCH_4 − $XCH_{4\,(+TROPPB\ var)}$ [ppb]	1 ± 2	0.1 ± 0.2
b) Stratosphere		
simple obs. XCH_4 − $XCH_{4(no\_str)}$ [ppb]	−37 ± 5	−26 ± 5
ACTM − CAMS [ppb]	−138 ± 9	−165 ± 15
ACTM − CAMSinv [ppb]	23 ± 5	24 ± 7

3.3.3 Stratospheric uncertainty

CH_4 shows variations in the stratosphere due to its reactions with excited oxygen (O(^{1}D)), OH and chlorine radicals (Saunois et al., 2020), which is represented in each model differently. GOSAT NIES CH_4 observations have a higher sensitivity in the stratospheric column as compared to CO_2 (averaging kernel >0.8 in the stratosphere, **Appendix A, Fig. A~~1~~2**). Therefore, the

shape and value of the modelled stratospheric CH$_4$ column impact the derived column-averaged dry-air mole fractions more than those for CO$_2$.

300 In the first step, we used the simple obs. XCH$_4$ to test the sensitivity of the stratospheric column on the derived XCH$_4$. We extrapolated CONTRAIL aircraft data through the TROPPB and the stratosphere up to 0.0128 hPa. XCH$_4$ calculated from profiles without considering the stratosphere was higher than the simple obs. XCH$_4$ by 37 ± 5 ppb (2.0 ± 0.3 %) and 26 ± 5 ppb (1.4 ± 0.3 %) at 30–40° N and 20–30° N, respectively (**Table 2**), which confirms the importance of the stratospheric column to derive XCH$_4$ correctly.

305 In the second step, we assessed the uncertainty of the stratospheric model. We calculated the difference MIROC4-ACTM − CAMS and MIROC4-ACTM − CAMSinv of the monthly averaged data above the TROPPB. ~~Then~~For that, we interpolated the MIROC4-ACTM data with its higher resolved pressure grid on that of the CAMS and CAMSinv data, respectively (**section 2.3**). CAMS was positively biased by 138 ± 9 ppb, and 165 ± 15 ppb at 30–40° N and 20–30° N, respectively (**Table 2, Appendix A, Fig. A~~3~~2 (a), (b)**). In contrast, the total average difference between MIROC4-ACTM and CAMSinv

310 was small as 23 ± 5 ppb, and 24 ± 7 ppb at 30–40° N and 20–30° N, respectively. In addition, the difference MIROC4-ACTM − CAMSinv depends on the season. The highest average difference occurred in June (30–40° N: 37 ± 6 ppb, 20–30° N: 44 ± 3 ppb), the lowest in October (4 ± 0.6 ppb) at 30–40° N, and January (5 ± 5 ppb) and February (3 ± 13 ppb) at 20–30° N (**Appendix A, Fig. A~~2~~3 (c), (d)**). A large positive stratospheric CH$_4$ bias of around 200 ppb of CAMS was recently reported by Agustí-Panareda et al. (2023), consistent with our observations. They suggest that uncertainties

315 associated with the stratospheric chemical loss of CH$_4$ are the largest contributor to that bias. Compared to CAMS, both the MIROC4-ACTM and CAMSinv ~~use optimized atmospheric transport models and~~ account for chemical losses in the stratosphere. Additionally, MIROC4-ACTM uses an optimized atmospheric transport model (Patra et al., 2018). The seasonality of the difference MIROC4-ACTM − CAMSinv indicates that the seasonal dependent chemical loss of CH$_4$ and/or meridional transport processes are modelled differently in both models.

320 Based on the total average difference between the latter 2 models, we added a $\pm$ 24 ppb uncertainty to the stratospheric column of the constructed CH$_4$ profile. The impact of the three stratospheric models on the calculated XCH$_4$ using this uncertainty is discussed in **section 4.2**.

4 Results and Discussion

4.1 Evaluation of the approaches

325 **Figure 3** shows the temporal variation of the XCH$_4$ calculated for the two selected latitude ranges (g1 = 30–40° N, g2 = 20–30° N) using approach 1 (simple obs. XCH$_4$), approach 2 (obs. XCH$_4$), and approach 3 (blended obs. XCH$_4$). For the period 2014 to mid-2017, we obtained 20 and 31 monthly averaged XCH$_4$ at the latitude ranges 30–40° N and 20–30° N, respectively. The uncertainty range of the simple obs. XCH$_4$ (22 ppb) is by 2 ppb and ~~5~~6 ppb larger than those of the obs. XCH$_4$ (20 ppb) and blended obs. XCH$_4$ (1~~7~~6 ppb), respectively (**section 3.3**). Furthermore, the difference between the latter

330   2 approaches is as small as 1 ± 3 ppb (blended obs. XCH_4 − obs. XCH_4) at both latitude ranges. In contrast, the difference between simple and blended obs. XCH_4 shows a variability of 2 ± 11 ppb and 4 ± 9 ppb at 30–40° N and 20–30° N, respectively.
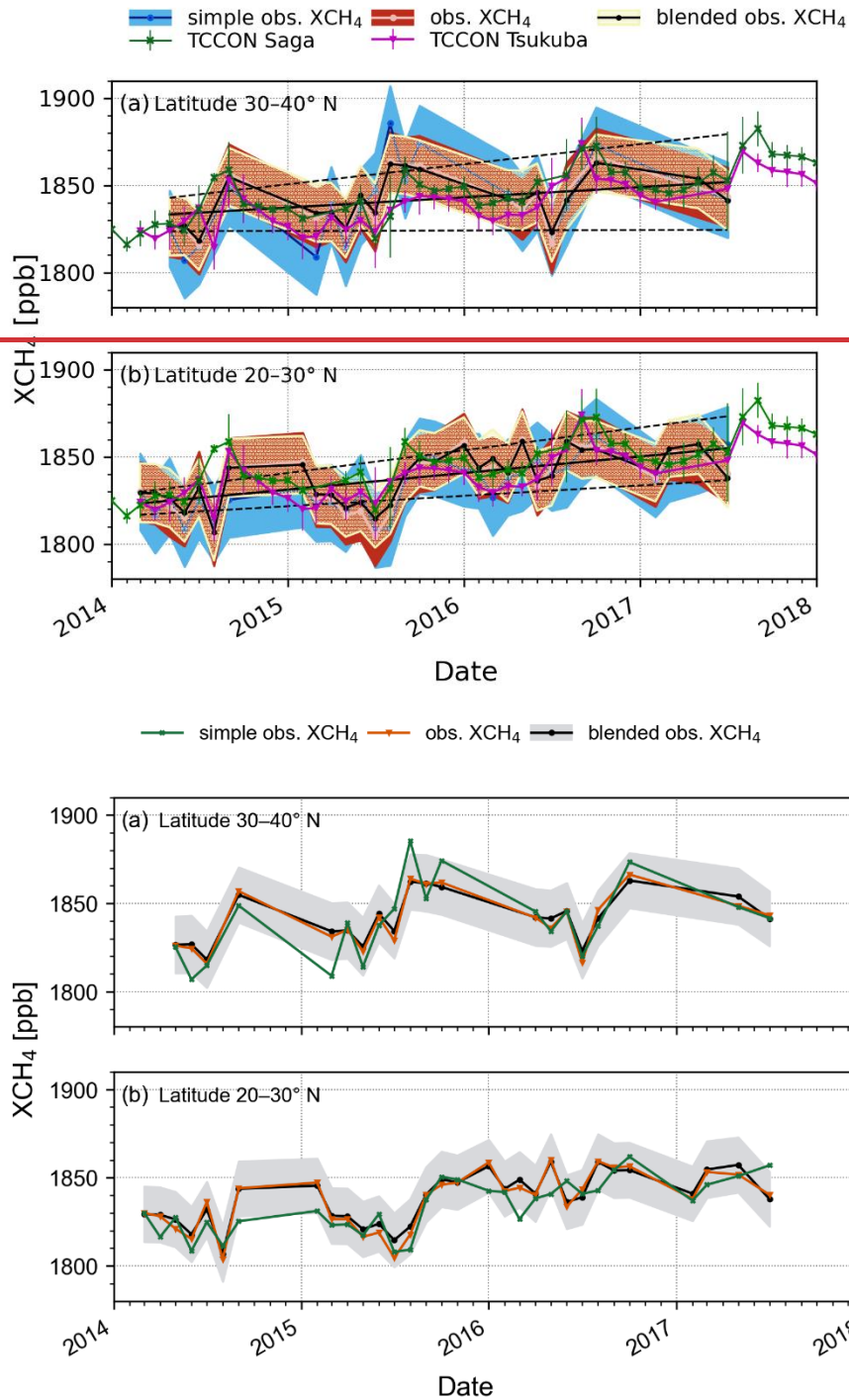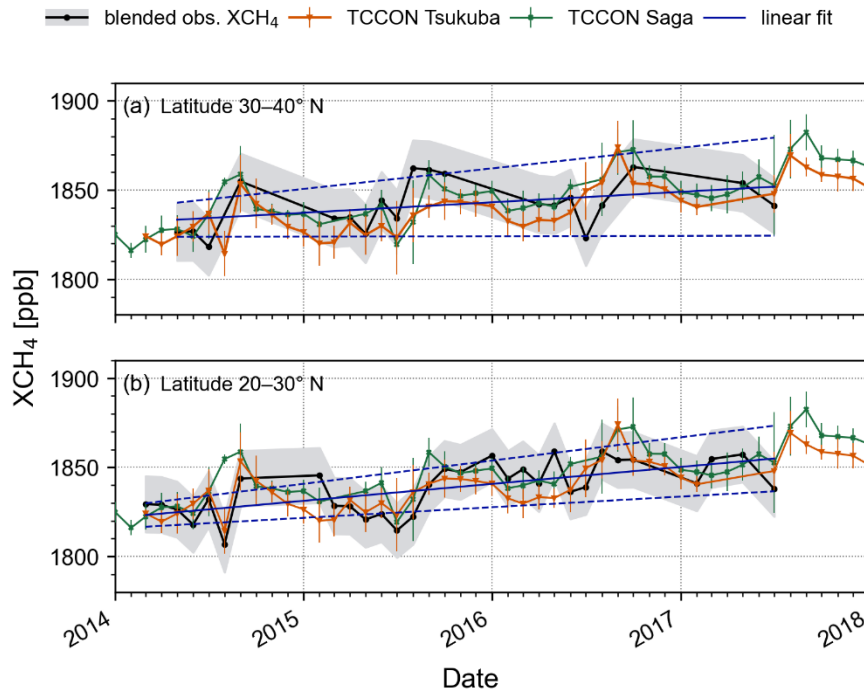
Figure 3: Temporal variation of monthly averaged XCH₄ obtained by approach 1 (simple obs. XCH₄, green), approach 2 (obs. XCH₄, orange), and approach 3 (blended obs. XCH₄, black) at the latitude range 30–40° N (a) and 20–30° N (b). The uncertainty ranges are 22

ppb, 20 ppb, and 16 ppb for approach 1, 2, and 3 respectively. Only the 16 ppb uncertainty range of approach 3 is shown as grey area. Other uncertainty ranges are omitted for readability.

340 ~~**Figure 3:** Temporal variation of monthly averaged XCH4 obtained by approach 1 (simple obs. XCH4, red), approach 2 (obs. XCH4, blue), and approach 3 (blended obs. XCH4, black), and from the TCCON station in Saga (green) and Tsukuba (magenta) at the latitude range 30–40° N (a) and 20–30° N (b). Shaded areas are the uncertainty ranges of the approaches; error bars are the standard deviations of TCCON. Also shown is the linear least-square regression (thick black line) with a 90% confidence interval on the slope and intercept (black dashed line) of approach 3.~~

345 To assess the correctness of the XCH4 datasets, we compare our data at both latitude ranges with the monthly averaged XCH4 data (version GGG2020) obtained from the nearest ground based TCCON stations in Tsukuba (36.05° N, 140.12° E, Morino et al., 2022) and Saga (33.24° N, 130.29° E, Shiomi et al., 2022) **(Fig. 1, ~~3~~4)**. Compared to Tsukuba, Saga is influenced by the continental outflow of airmasses from East Asia. It is noted that the distance of about 1300 km between the TCCON stations and the center of g2 is large. Considering that there are no strong CH4 sources over the open ocean at g2,

350 the comparison gives us an indication about the applicability of the datasets.


Figure 4: Temporal variation of monthly averaged XCH4 obtained by approach 3 (blended obs. XCH4, black), and from the TCCON station in Saga (green) and Tsukuba (orange) at the latitude range 30–40° N (a) and 20–30° N (b). The grey area is the 16 ppb uncertainty range of approach 3; error bars are the standard deviations of TCCON. Also shown is the linear least-square regression (deep blue line)
355 with a 90% confidence interval on the slope and intercept (deep blue dashed line) of approach 3.

16

For readability, only the blended obs. XCH$_4$ in comparison with the TCCON stations is shown in Fig. 4. By looking at the averaged difference at g1, XCH$_4$ from Tsukuba was lower than that derived from our approaches with −3 ± 20 ppb, −3 ± 14 ppb, and −4 ± 13 ppb for approach 1, 2, and 3, respectively. In contrast, XCH$_4$ from Saga was higher and showed better

360   agreement with differences of 1 ± 20 ppb for approach 1, and 1 ± 12 ppb for approach 2 and 3. At g2, XCH$_4$ from Tsukuba matches our data better than that from Saga with 3 ± 11 ppb, 0 ± 12 ppb, and −1 ± 11 ppb for approach 1, 2, and 3. Saga showed a higher discrepancy of 9 ± 12 ppb, 6 ± 14 ppb, and 5 ± 14 ppb for the respective approaches. The similarity between XCH$_4$ from our approaches and Saga at g1, and Tsukuba at g2, indicates that the ocean area at 30–40° N (g1) is rather influenced by the continental outflow of CH$_4$ from Asia, while 20–30° N (g2) showed cleaner conditions.

365   Given the ~~lower uncertainty range and~~ lower maximal possible averaged difference between TCCON and approach 2 and 3 compared to approach 1, and given the lowest uncertainty range of approach 3, the latter ~~2~~ approach~~es are~~is preferable for future applications. ~~A clear advantage of the more elaborate approach 3 is not seen but might become clearer with extended in situ datasets.~~ Therefore, we use the results of approach 3 (blended obs. XCH$_4$) for further discussion.

4.2 Evaluation of the stratospheric model

370   **Figure ~~4~~5** shows the comparison of the blended obs. XCH$_4$ (approach 3) using the MIROC4-ACTM, CAMS, and CAMSinv for the stratospheric column (**section 3.3.3**), denoted as ACTM$_{XCH4}$, CAMS$_{XCH4}$, and CAMSinv$_{XCH4}$. Using ACTM$_{XCH4}$ as reference, CAMS$_{XCH4}$ is highly biased at both latitude ranges by 12 ± 5 ppb (0.6 ± 0.2%) in total. In contrast, CAMSinv$_{XCH4}$ shows a small negative total bias of −5 ± 3 ppb (−0.3 ± 0.2%). CAMS has a known large positive stratospheric CH$_4$ bias (Agustí-Panareda et al., 2023). MIROC4-ACTM and CAMS$_{inv}$ account for stratospheric CH$_4$ loss and the modelled

375   stratosphere is comparable as discussed in **section 3.3.3**. The similarity of the ACTM$_{XCH4}$ and CAMS$_{invXCH4}$~~the latter two results~~ and their differences to CAMS$_{XCH4}$ indicate ~~shows~~ the strong impact of the stratospheric part on the derived XCH$_4$ and highlights the importance to make an appropriate model choice (**compare section 3.3.3**). Considering the large uncertainty of CAMS and the fact that the other two products are better optimized for modelling CH$_4$ in the stratosphere~~Based on our observations~~, we suggest using either the MIROC4-ACTM or CAMSinv to model the stratospheric

380   column. In the following, we use the ACTM$_{XCH4}$ to demonstrate the applicability of the dataset for satellite evaluation. However, for the operational application in future, the public available CAMSinv might be the better choice until the MIROC4-ACTM will be available in near-real time.
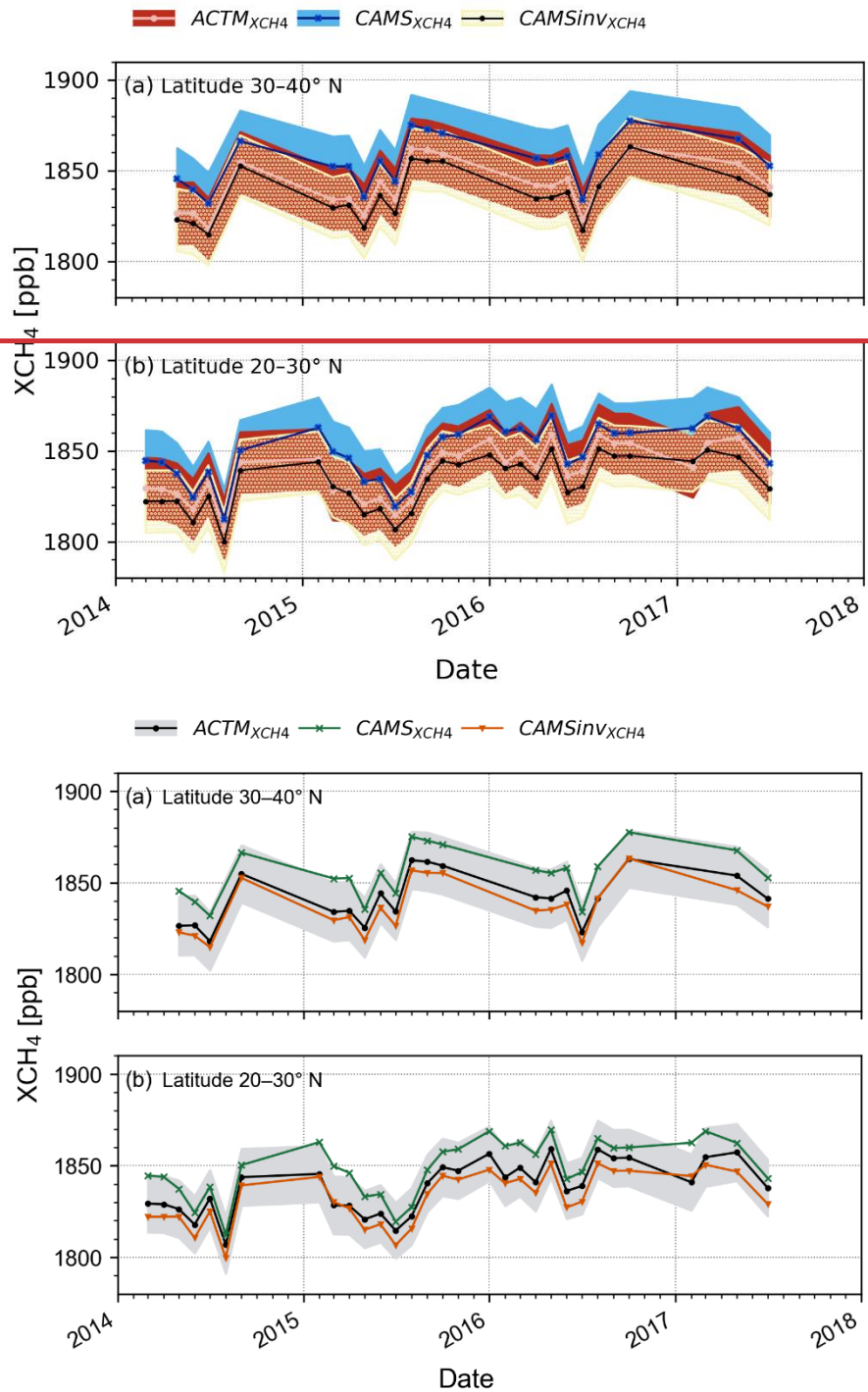
Figure 4<u>5</u>: Comparison between the blended obs. XCH4 (approach 3) derived from CH4 profiles using the MIROC4-ACTM (ACTM_XCH4, ~~red~~<u>black</u>), CAMS (CAMS_XCH4, ~~blue~~<u>green</u>), and CAMSinv (CAMSinv_XCH4, ~~black~~<u>orange</u>) for the stratospheric column at the latitude range

18

30–40° N (a) and 20–30° N (b). ~~Shaded areas are t~~The uncertainty range of all results is 16 ppb~~s~~. The grey area is the uncertainty of ACTM$_{XCH4}$. Uncertainty ranges of the other results are not shown for readability.

4.3 Applicability of observation-based XCH$_4$

390   In the following we want to demonstrate the applicability of the in situ derived XCH$_4$ datasets for carbon cycles studies by analyzing the seasonal variation of XCH$_4$ over the ocean, and for satellite evaluation. We will focus on the blended obs. XCH$_4$.

4.3.1 Seasonal variation

Figure 3 shows that all three approaches follow similar temporal variations and trends. At 30–40° N, a rough seasonal cycle
395   with lower values between winter and summer (minima in July) and maxima between August to October is seen. The column observations of CH$_4$ are consistent with northern hemispherical surface observations (e.g., Dlugokencky et al., 1995). Minima between July and August and maxima in the period winter to spring have been observed at the lower troposphere by aircraft and ground based stations in Japan (Umezawa et al., 2014; Tohjima et al., 2002). The seasonal characteristics are explained by the interaction between air mass origin and atmospheric OH concentration. In summer,
400   south-easterly air masses from CH$_4$ source-free regions of the Pacific Ocean and the surrounding of Japan are dominant. In addition, the OH concentration is highest in summer, which leads to enhanced CH$_4$ removal from the atmosphere. In winter, when the removal through OH oxidation is lowest, prevailing north-westerly winds bring CH$_4$ rich air masses from China and Siberia (Umezawa et al., 2014; Tohjima et al., 2002). This explains the larger CH$_4$ concentration during that period.

At 20–30° N, lower values are obvious from winter to the end of summer (August) in 2015, but in 2016, it is not as clear as
405   at 30–40° N. **Figure ~~3~~4** also shows the linear least-squares regression with 90% confidence interval on the slope and intercept of approach 3. At 30–40° N, the annual increase in XCH$_4$ is within the uncertainty range with 9 ± 9 ppb for the simple obs. XCH$_4$, and 6 ± 6 ppb for the other two approaches. In contrast, at 20–30° N, the annual increase is significant with 11 ± 3 ppb for the simple obs. XCH$_4$, and 10 ± 4 and 9 ± 4 ppb for the obs. and blended obs. XCH$_4$. The higher summertime values in 2016 contribute to the difference in the growth rates at 20–30° N. Similar strong growth rates have
410   been reported for the global atmospheric CH$_4$ concentration between 2014 to 2017 with a peak in 2014 of 13 ppb, and a minimum in 2016 of 7 ppb (Nisbet et al., 2019). It is noted that limited and uneven sampled in situ data during each month might cause an artificial difference of the growth rates between the latitude ranges. However, given a lower growth rate at the higher latitude range combined with a higher similarity of the blended obs. XCH$_4$ with those XCH$_4$ influenced by the Asian emission outflow at Saga (**chapter 4.1**), we can suggest that the interaction between anthropogenic emissions might
415   have led to increased OH concentrations, consequently higher CH$_4$ removal rates near to the Japanese East coast (**Fig. 1**), and therefore causing a slower annual growth. Or it might indicate that compared to 20–30° N, the higher latitude range is affected by the decreasing trend in CH$_4$ emission from Japan (Ito et al., 2023).

A possible explanation for the observed increased summertime XCH$_4$ values in 2016 can be the characteristics of the prevailing southerly winds in that season. In the years 2015 to 2016, a strong El Niño event took place, which is linked to

420   extreme heat and drought, and consequently to increased biomass burning in tropical regions (Bousquet et al., 2006; Parker et al., 2016; Whitburn et al., 2016). Smoldering combustion in peatland fires can release large amounts of CH$_4$ (Bousquet et al., 2006; Parker et al., 2016). Using GOSAT observations, Parker et al. (2016) reported an enhancement of XCH$_4$ of 35 ppb above background conditions over Indonesian peatland fires at the end of 2015. Furthermore, Zhang et al. (2018) demonstrated that enhanced CH$_4$ emissions from wetland areas from January through May 2016 are related to the strong El

425   Niño which provides an explanation for a rise of the atmospheric CH$_4$ growth rate. Therefore, southerly air masses of high CH$_4$ concentration might have affected the study region. Our observations demonstrate the capability of the ship-aircraft based dataset to capture seasonal variations and climatological events like the El Niño.

4.3.2 Satellite evaluation

Figure ~~5~~6 shows the temporal variation of the blended obs. XCH$_4$ (ACTM$_{XCH4}$) in comparison with XCH$_4$ from GOSAT

430   observations using the NIES, RemoTeC, and OCFP retrieval (**section 2.4**). The retrievals mostly lie in the uncertainty range (1~~7~~6 ppb) of the blended obs. XCH$_4$. The difference "blended obs. XCH$_4$ − NIES" is −0.04 ± 12.65 ppb and −0.04 ± 13.32 ppb at 30–40° N and 20–30° N, respectively. The high standard deviations are similar to that reported for the difference between NIES and TCCON ocean data in the data release note of the NIES GOSAT project (NIES GOSAT Project, 2020). The difference between blended obs. XCH$_4$ and RemoTeC show a larger average discrepancy of 11.8 ± 16.2 ppb and 12.1 ±

435   8.1 ppb but with smaller standard deviation at 20–30° N. At 30–40° N, OCFP provides almost no valid data. The difference is 2.2 ± 21.0 ppb. At 20–30° N, the difference "blended obs. XCH$_4$ – OCFP" of 10.3 ± 9.6 ppb is similar to the difference of RemoTeC. The smaller standard deviations of RemoTeC and OCFP suggest rather a systematic offset at that latitude range. The higher difference compared to NIES can arise from the choice of a priori profiles and column averaging kernel in the retrieval and their choice in calculation of the blended obs. XCH$_4$ (**section 3.2**). To clarify if the offset of RemoTeC and

440   OCFP is a true regional or ocean bias, further analyses are needed in future.
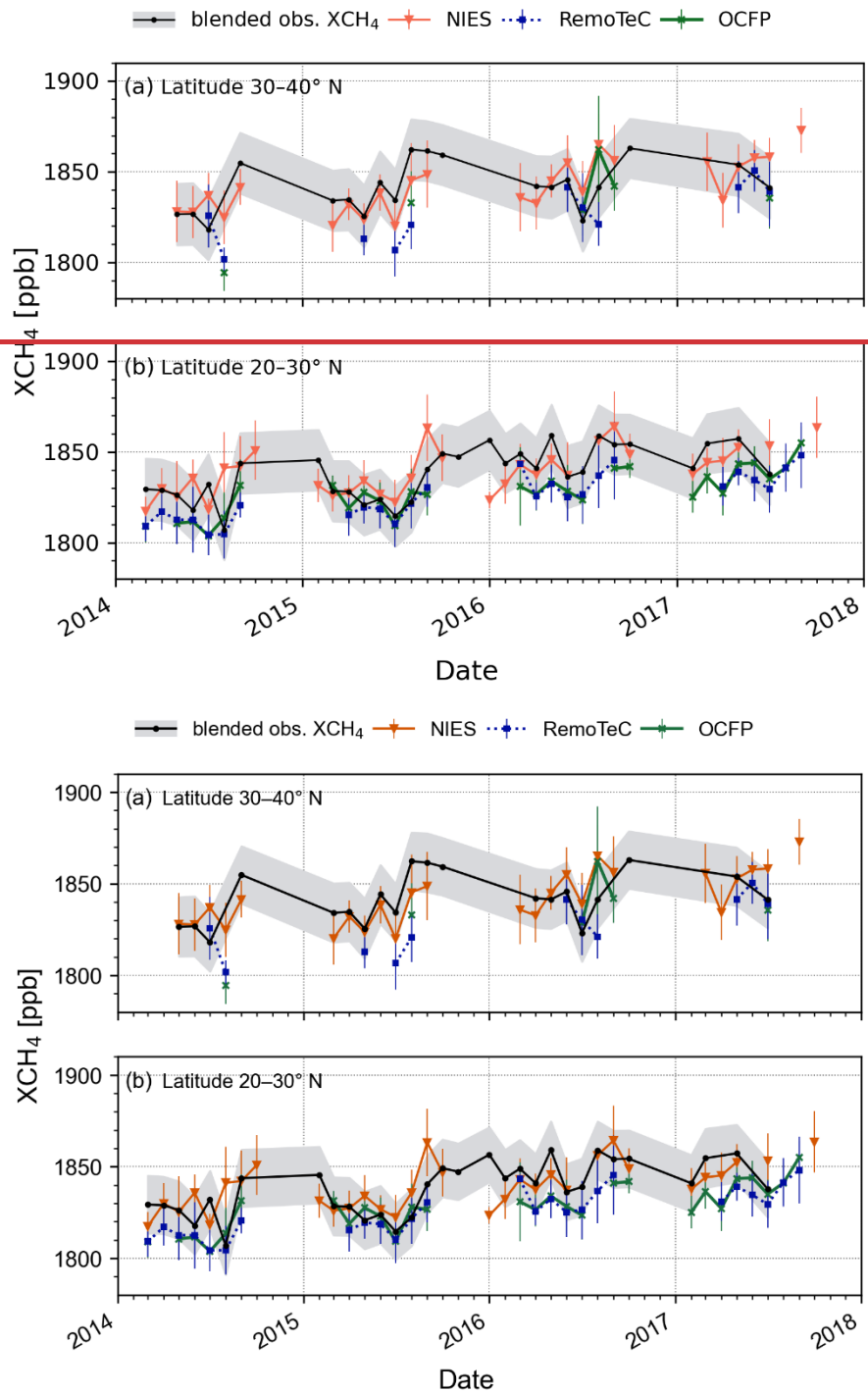
Figure 65: Temporal variation of the blended obs. XCH4 (ACTM$_{XCH4}$, black) in comparison with GOSAT XCH4 retrievals from NIES (~~red~~orange), RemoTeC (blue), and OCFP (green) at the latitude range 30–40° N (a) and 20–30° N (b). The grey area is the 16 ppb uncertainty of the blended obs. XCH4.

5 Summary and Conclusion

As reference dataset for satellite validation and carbon cycle studies, we investigated three different approaches to derive column-averaged dry-air mole fractions of CH_4 (XCH_4) over oceans by integrating commercial ship and aircraft observations. The study focused on the latitude ranges 30–40° N and 20–30° N at the longitude 130–150° E between the years 2014 and 2018. Approach 1 used simple linear inter- and extrapolation between ship and aircraft data of the upper troposphere; approach 2 used additional aircraft data of the middle troposphere, and approach 3 added model results between the middle and upper tropospheric aircraft observations. All three approaches used model results for the stratospheric column.

Uncertainties of the calculated XCH_4 were reduced by 2~~5~~ ppb and 6 ppb from 22 ppb (approach 1) to ~~17~~20 ppb for approach 2 and 16 ppb for approach 3. XCH_4 derived from approach 2 and 3 were similar within 1 ± 3 ppb. The difference between approach 3 and 1 was about 30% higher. At 30–40° N, XCH_4 data of the TCCON station Saga, influenced by the Asian continental outflow, showed a better agreement with our approaches (within 1 ± 20 ppb for approach 1, 1 ± 12 ppb for approach 2 and 3) than that from Tsukuba (which was lower by −3 ± 20 ppb, −3 ± 14 ppb, and −4 ± 13 ppb than approach 1, 2, and 3). At 20–30° N, better agreement was found with TCCON data of Tsukuba (difference of Tsukuba: 3 ± 11 ppb, 0 ± 12 ppb, and −1 ± 11 ppb, and of Saga of: 9 ± 12 ppb, 6 ± 14 ppb, and 5 ± 14 ppb, for approach 1, 2, and 3). These observations indicate a stronger impact of continental emissions on the higher latitudinal study area. Based on the lowest uncertainty and difference towards TCCON, ~~we selected~~ approach 3, defined as blended observation-based XCH_4 (blended obs. XCH_4), is the most suitable for evaluating satellite observations over oceans.

Applying approach 3, we found that omitting the stratospheric column in the CH_4 profile impacts the derived blended obs. XCH_4 by about 2%, which is significantly higher than the corresponding impact on the derived XCO_2 of our previous study (<0.1%). Using CAMSinv or MIROC4-ACTM for the stratospheric column, the derived blended obs. XCH_4 was similar within 8 ppb (0.3 ± 0.2%). Using CAMS instead of MIROC4-ACTM, the blended obs. XCH_4 was higher biased by 12 ± 5 ppb (0.6 ± 0.2%). ~~Since~~ MIROC4-ACTM and CAMSinv ~~use optimized transport models and~~ consider chemical losses in the stratosphere, where MIROC4-ACTM additionally uses an optimized atmospheric transport model. We conclude that for accurately deriving XCH_4, a well modelled stratosphere is necessary that includes CH_4 sinks. Therefore, ~~we propose~~ either ~~to use~~ CAMSinv or MIROC4-ACTM, is suitable for our approach of which CAMSinv is publicly available.

The temporal variation of the blended obs. XCH_4 showed minima in summer (July) and maxima between August and October, and an annual growth rate between 6 and 10 ppb, consistent with previous studies. In 2016, we observed a weaker summertime minimum and suggest that this is the result of the strong 2015/2016 El Niño event which was related to higher CH_4 emissions and growth rates. The comparison of our results with GOSAT XCH_4 retrievals from NIES showed strong scatter of the differences with −0.04 ± 13 ppb. In contrast, RemoTeC and OCFP showed a larger but rather systematic negative bias of −12.1 ± 8.1 ppb and −10.3 ± 9.6 ppb at 20–30° N, which is likely related to differences in a priori profiles

and column averaging kernels of the retrieval. These observations show that using the blended obs. XCH$_4$ dataset, CH$_4$ trends and seasonal variations can be detected, and satellite observations evaluated.

480 Having an uncertainty range lower than the mission targets of GOSAT and TROPOMI, the accuracy of satellite derived XCH$_4$ over oceans can be accessed by our best approach 3. While the blended obs. XCH$_4$ dataset is not suitable for detecting small scale variations of CH$_4$ like those from point sources and sinks, spatial pattern and large-scale long-term trends can be evaluated and used for carbon cycle studies. Furthermore, our ship-aircraft based approach has the potential to quickly create long-term dataset in areas where other highly precise reference data, such as from measurement campaigns like HIPPO

485 flights or TCCON stations, are not available. Uncertainties and limitations caused by ~~We are aware that our results are based on very~~ limited in situ data will be reduced ~~, and conclusions made from the seasonal variation and the quantitative descriptions need to be taken carefully. We want to stress that~~ in the near future. This includes the re-start of aircraft observations by CONTRAIL over the western Pacific Ocean ~~will re-start~~, probably within the next 2 years, and the spatial extension. ~~Together with data~~ of other aircraft projects like that of the In-service Aircraft for a Global Observing System

490 (IAGOS) project. ~~, CH$_4$ data of the upper troposphere will increase rapidly. However, additional ship routes would be beneficial. Despite the current limitations, our study could demonstrate the applicability of the new dataset as reference for carbon cycle studies and for satellite evaluation over oceans.~~ As a complement to established validation networks, we can contribute with our ship-aircraft derived XCH$_4$ dataset to the validation of TROPOMI, GOSAT-GW and other upcoming satellite missions in future.

495 **Appendix A**
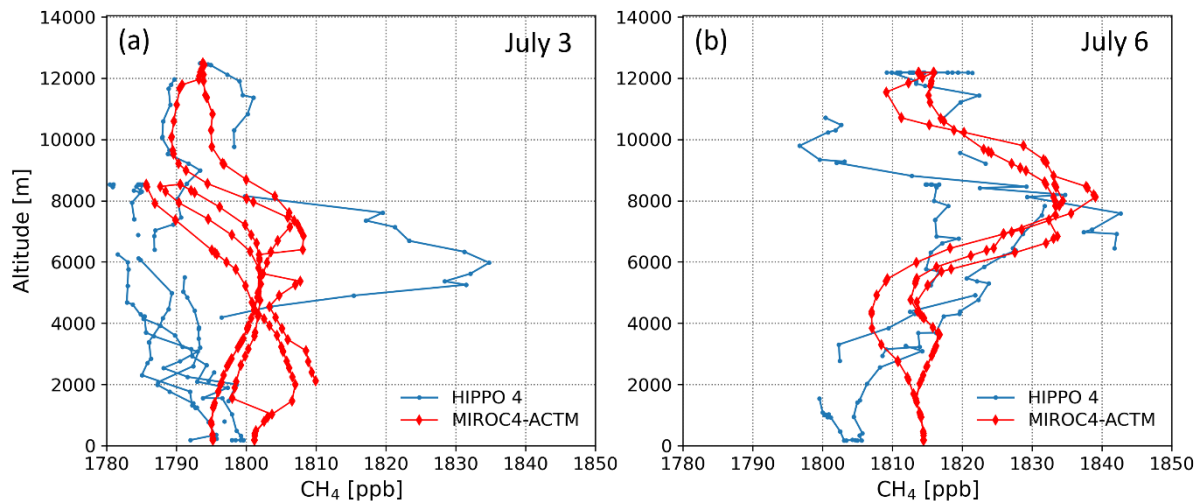
Figure A1: Comparison between HIPPO 4 (blue) and MIROC4-ACTM profiles (red) on July 3 (a) and 6 (b), 2011.
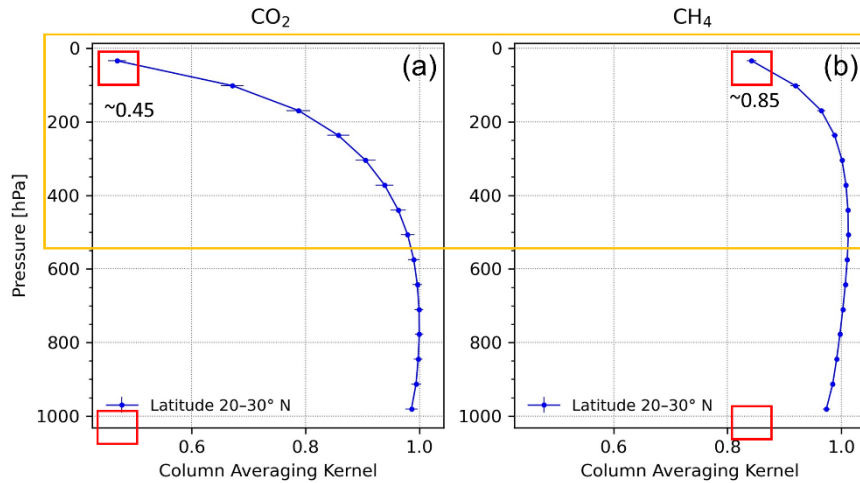
Figure A2̶1̶: The GOSAT NIES column averaging kernel (ak) in dependence of the pressure for CO_2 (a) and CH_4 (b) at the latitude range 20–30° N. The yellow square indicates the area of major differences; the red squares emphasize the difference in the ak value at the lowest pressure of 34 hPa. Compared to the ak of CO_2, the impact of the CH_4 profile on the calculated XCH_4 is high below the tropopause (400 – 200 hPa) and at the stratospheric part.
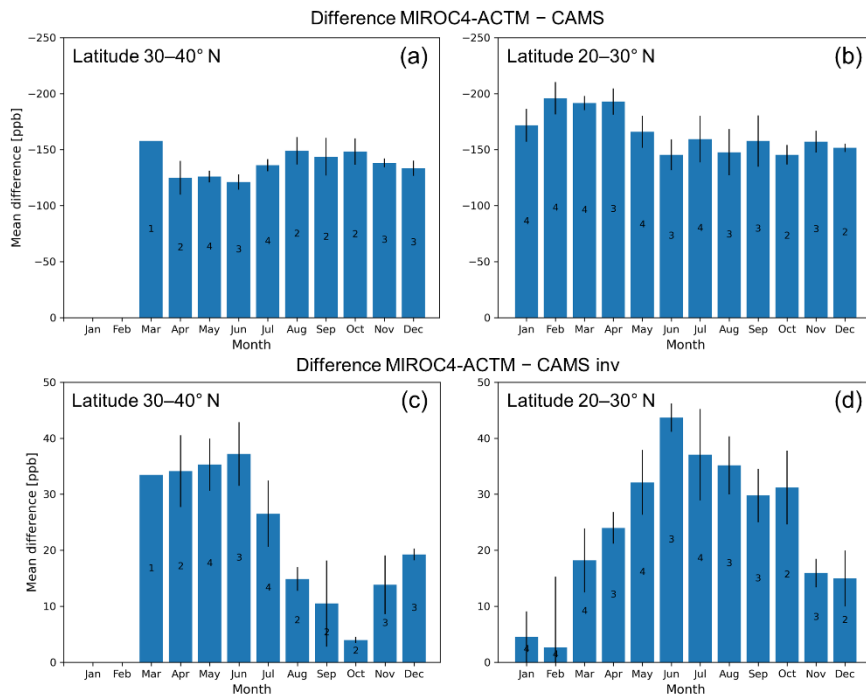
Figure A3̶2̶: Monthly averaged difference between MIROC4-ACTM and CAMS (a), (b), and MIROC4-ACTM and CAMSinv (c), (d) at the latitude range 30–40° N and 20–30° N, respectively. Error bars are the standard deviation of the monthly averages. Numbers inside the bars correspond to the number of mean values per month.

24
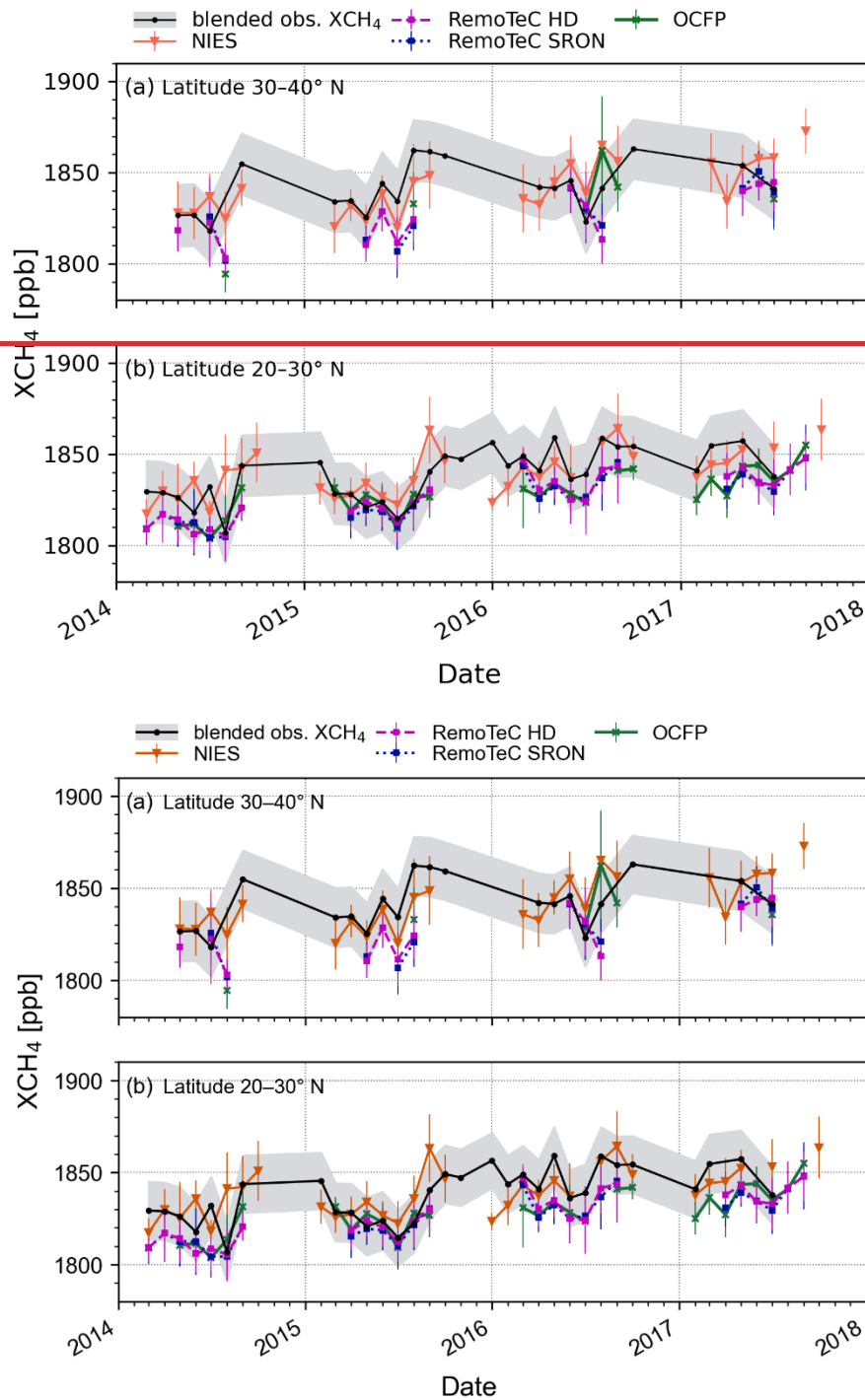
Figure A43: Temporal variation of the blended obs. XCH4 (ACTM$_{XCH4}$, black) in comparison with GOSAT XCH4 retrievals from NIES (orangered), RemoTeC Heidelberg (HD) (magenta), RemoTeC SRON (blue), and OCFP (green) at the latitude range g1 = 30–40° N (a) and g2 = 20–30° N (b). The grey area is the 16 ppb uncertainty range of the blended obs. XCH4. The difference RemoTeC HD −

510

25

RemoTeC SRON is −0.4 ± 4.4 ppb and 1.6 ± 3.0 ppb (mean difference ± standard deviation of differences) at g1 and g2, respectively. The average number of valid retrievals per month for RemoTeC HD (g1: 20 ± 14 ppb, 13 months; g2: 50 ± 29 ppb, 24 months) is larger than for RemoTeC SRON (g1: 24 ± 16 ppb, 11 months; g2: 41 ± 24 ppb, 24 months).

Data availability

The GOSAT data of the NIES retrieval algorithm are available from the GOSAT Project website of the National Institute for Environmental Studies (NIES) at https://data2.gosat.nies.go.jp/index_en.html, last access: 17 May 2023.

GOSAT data of the RemoTeC full-physics retrieval from SRON (SRFP) and the OCO full-physics retrieval by the University of Leicester (OCFP) are available from the Copernicus Climate Change Service, Climate Data Store at https://doi.org/10.24381/cds.b25419f8, accessed on 17 May 2023.

XCH_4 data of the RemoTeC full-physics retrieval by Heidelberg University are available upon request (andre.butz@iup.uni-heidelberg.de).

The CH_4 mole fraction data of CONTRAIL (https://doi.org/10.17595/20190828.001, Machida et al., 2019) are available from the Global Environmental Database (GED) of NIES (https://db.cger.nies.go.jp/ged/en/links/index.html?id=link1, GED, 2022). CONTRAIL data are also available from the World Data Center for Green-house Gases (WDCGG) at https://gaw.kishou.go.jp/, last access: 17 May 2023. NIES SOOP CH_4 will be released at the GED by the end of 2023. CAMS and CAMSinv data are available from the Atmosphere Data Store operated by the European Centre for Medium-Range Weather Forecasts at https://ads.atmosphere.copernicus.eu, last access: 17 May 2023.

TCCON data are available from the TCCON Data Archive hosted by CaltechDATA at https://tccondata.org, last access: 17 May 2023.

MIROC4-ACTM concentration data are available upon request (prabir@jamstec.go.jp).

Supplement

Data used in this study accompany the article.

Author contribution

The study was designed by HT. Data analyses were made by AM. MIROC4-ACTM data were provided by PKP. ~~CAMSinv data were provided by CWO.~~ Extensive discussions were made by AM, HT, TS, PKP. The paper was written, edited, and proofed by all the authors.

Competing interests

26

The co-author André Butz is an Executive editor of the editorial board of the AMT. The peer-review process was guided by an independent editor. The authors have no other competing interests to declare.

References

Agustí-Panareda, A., Barré, J., Massart, S., Inness, A., Aben, I., Ades, M., Baier, B. C., Balsamo, G., Borsdorff, T., Bousserez, N., Boussetta, S., Buchwitz, M., Cantarello, L., Crevoisier, C., Engelen, R., Eskes, H., Flemming, J., Garrigues, S., Hasekamp, O., Huijnen, V., Jones, L., Kipling, Z., Langerock, B., McNorton, J., Meilhac, N., Noël, S., Parrington, M., Peuch, V.-H., Ramonet, M., Razinger, M., Reuter, M., Ribas, R., Suttie, M., Sweeney, C., Tarniewicz, J., and Wu, L.: Technical note: The CAMS greenhouse gas reanalysis from 2003 to 2020, Atmos Chem Phys, 23, 3829–3859, https://doi.org/10.5194/acp-23-3829-2023, 2023.

Boesch, H. and Noia, A. Di: Algorithm Theoretical Basis Document (ATBD) – ANNEX A for products CO2_GOS_OCFP (v7.3), CH4_GOS_OCFP (v7.3) & CH4_GOS_OCPR (v9.0) (CDR6, 2009-2021), 1–40, 2023.

Bousquet, P., Ciais, P., Miller, J. B., Dlugokencky, E. J., Hauglustaine, D. A., Prigent, C., Van Der Werf, G. R., Peylin, P., Brunke, E. G., Carouge, C., Langenfelds, R. L., Lathière, J., Papa, F., Ramonet, M., Schmidt, M., Steele, L. P., Tyler, S. C., and White, J.: Contribution of anthropogenic and natural sources to atmospheric methane variability, Nature, 443, 439–443, https://doi.org/10.1038/nature05132, 2006.

Bovensmann, H., Burrows, J. P., Buchwitz, M., Frerick, J., Noël, S., Rozanov, V. V., Chance, K. V., and Goede, A. P. H.: SCIAMACHY: Mission Objectives and Measurement Modes, J. Atmos. Sci., 56, 127–150, https://doi.org/10.1175/1520-0469(1999)056<0127:SMOAMM>2.0.CO;2, 1999.

Buchwitz, M., Reuter, M., Schneising, O., Hewson, W., Detmers, R. G., Boesch, H., Hasekamp, O. P., Aben, I., Bovensmann, H., Burrows, J. P., Butz, A., Chevallier, F., Dils, B., Frankenberg, C., Heymann, J., Lichtenberg, G., De Mazière, M., Notholt, J., Parker, R., Warneke, T., Zehner, C., Griffith, D. W. T., Deutscher, N. M., Kuze, A., Suto, H., and Wunch, D.: Global satellite observations of column-averaged carbon dioxide and methane: The GHG-CCI XCO_2 and XCH_4 CRDP3 data set, Remote Sens. Environ., 203, 276–295, https://doi.org/10.1016/j.rse.2016.12.027, 2017.

Buchwitz, M., Chevallier, F., and Marshall, J.: User Requirements Document (URD) - Greenhouse Gases (GHG), Simulation, 42, 2020.

Butz, A., Guerlet, S., Hasekamp, O., Schepers, D., Galli, A., Aben, I., Frankenberg, C., Hartmann, J. M., Tran, H., Kuze, A., Keppel-Aleks, G., Toon, G., Wunch, D., Wennberg, P., Deutscher, N., Griffith, D., MacAtangay, R., Messerschmidt, J., Notholt, J., and Warneke, T.: Toward accurate CO_2 and CH_4 observations from GOSAT, Geophys. Res. Lett., 38, 2–7, https://doi.org/10.1029/2011GL047888, 2011.

Canadell, J. G., Monteiro, P. M. S., Costa, M. H., Cunha, L. C. da, Cox, P. M., Eliseev, A. V., Henson, S., Ishii, M., Jaccard, S., Koven, C., Lohila, A., Patra, P. K., Piao, S., Rogelj, J., Syampungani, S., Zaehle, S., and Zickfeld, K.: Global Carbon and other Biogeochemical Cycles and Feedbacks. In: Climate Change 2021: The Physical Science Basis. Contribution of Working Group I to the Sixth Assessment Report of the Intergovernmental Panel on Climate Change, edited by: Intergovernmental Panel on Climate Change, Cambridge University Press, Cambridge, 673–816 pp., https://doi.org/10.1017/9781009157896.007, 2021.

Connor, B. J., Boesch, H., Toon, G., Sen, B., Miller, C., and Crisp, D.: Orbiting Carbon Observatory: Inverse method and prospective error analysis, J. Geophys. Res. Atmos., 113, 1–14, https://doi.org/10.1029/2006JD008336, 2008.

Copernicus Climate Change Service, Climate Data Store, (2018): Methane data from 2002 to present derived from satellite observations,. Copernicus Climate Change Service (C3S) Climate Data Store (CDS), https://doi.org/10.24381/cds.b25419f8, 2018, accessed on 17 May 2023.

Dlugokencky, E. J.: Conversion of NOAA atmospheric dry air CH_4 mole fractions to a gravimetrically prepared standard scale, J. Geophys. Res., 110, D18306, https://doi.org/10.1029/2005JD006035, 2005.

Dlugokencky, E. J., Steele, L. P., Lang, P. M., and Masarie, K. A.: Atmospheric methane at Mauna Loa and Barrow observatories: presentation and analysis of in situ measurements, J. Geophys. Res., 100, https://doi.org/10.1029/95jd02460, 1995.

Dlugokencky, E. J., Bruhwiler, L., White, J. W. C., Emmons, L. K., Novelli, P. C., Montzka, S. A., Masarie, K. A., Lang, P. M., Crotwell, A. M., Miller, J. B., and Gatti, L. V.: Observational constraints on recent increases in the atmospheric CH_4 burden, Geophys. Res. Lett., 36, 3–7, https://doi.org/10.1029/2009GL039780, 2009.

Enyo, K. and Kadono, K.: Atmospheric CH_4 by Ryofu Maru, R/V Japan Meteorological Agency, dataset published as CH4_RYF_ ship-insitu_JMA_air-sampling at WDCGG, ver. 2021-06-24-0040, accessed on 5 December 2022.

ESA, European Space Agency: Sentinel-5 Precursor Calibration and Validation Plan for the Operational Phase, Issue 1, Revision 1, 26 pp., https://sentinel.esa.int/documents/247904/2474724/Sentinel-5P-Calibration-and-Validation-Plan.pdf, 2017, accessed on 28 November 2023.

Forster, P., Ramaswamy, V., Artaxo, P., Berntsen, T., Betts, R., Fahey, D. W., Haywood, J., Lean, J., Lowe, D. C., Myhre, G., Nganga, J., Prinn, R., Raga, G., Schulz, M., Dorland, R. Van.: Changes in Atmospheric Constituents and in Radiative Forcing. In: Climate Change 2007: The Physical Science Basis. Contribution of Working Group I to the Fourth Assessment Report of the Intergovernmental Panel on Climate Change, 129–234, 2007.

Frankenberg, C., Meirink, J. F., van Weele, M., Platt, U., and Wagner, T.: Assessing Methane Emissions from Global Space-Borne Observations, Science, 308, 1010–1014, https://doi.org/10.1126/science.1106644, 2005.

Guerlet, S., Butz, A., Schepers, D., Basu, S., Hasekamp, O. P., Kuze, A., Yokota, T., Blavier, J. F., Deutscher, N. M., Griffith, D. W. T., Hase, F., Kyro, E., Morino, I., Sherlock, V., Sussmann, R., Galli, A., and Aben, I.: Impact of aerosol and thin cirrus on retrieving and validating XCO_2 from GOSAT shortwave infrared measurements, J. Geophys. Res. Atmos., 118, 4887–4905, https://doi.org/10.1002/jgrd.50332, 2013.

Inness, A., Ades, M., Agustí-Panareda, A., Barr, J., Benedictow, A., Blechschmidt, A. M., Jose Dominguez, J., Engelen, R., Eskes, H., Flemming, J., Huijnen, V., Jones, L., Kipling, Z., Massart, S., Parrington, M., Peuch, V. H., Razinger, M., Remy, S., Schulz, M., and Suttie, M.: The CAMS reanalysis of atmospheric composition, Atmos. Chem. Phys., 19, 3515–3556, https://doi.org/10.5194/acp-19-3515-2019, 2019.

IPCC, 2021: Summary for Policymakers. In: Climate Change 2021: The Physical Science Basis. Contribution of Working Group I to the Sixth Assessment Report of the Intergovernmental Panel on Climate Change [Masson-Delmotte, V., P.

Zhai, A. Pirani, S.L. Connors, C. Péan, S. Berger, N. Caud, Y. Chen, L. Goldfarb, M.I. Gomis, M. Huang, K. Leitzell, E. Lonnoy, J.B.R. Matthews, T.K. Maycock, T. Waterfield, O. Yelekçi, R. Yu, and B. Zhou (eds.)]. Cambridge University Press, Cambridge, United Kingdom and New York, NY, USA, pp. 3−32, doi:10.1017/9781009157896.001, 2021.

Ito, A., Patra, P. K., and Umezawa, T.: Bottom-Up Evaluation of the Methane Budget in Asia and Its Subregions, Global Biogeochem Cycles, 37, https://doi.org/10.1029/2023gb007723, 2023.

Kirschke, S., Bousquet, P., Ciais, P., Saunois, M., Canadell, J. G., Dlugokencky, E. J., Bergamaschi, P., Bergmann, D., Blake, D. R., Bruhwiler, L., Cameron-Smith, P., Castaldi, S., Chevallier, F., Feng, L., Fraser, A., Heimann, M., Hodson, E. L., Houweling, S., Josse, B., Fraser, P. J., Krummel, P. B., Lamarque, J. F., Langenfelds, R. L., Le Quéré, C., Naik, V., O'doherty, S., Palmer, P. I., Pison, I., Plummer, D., Poulter, B., Prinn, R. G., Rigby, M., Ringeval, B., Santini, M., Schmidt, M., Shindell, D. T., Simpson, I. J., Spahni, R., Steele, L. P., Strode, S. A., Sudo, K., Szopa, S., Van Der Werf, G. R., Voulgarakis, A., Van Weele, M., Weiss, R. F., Williams, J. E., and Zeng, G.: Three decades of global methane sources and sinks, Nat. Geosci., 6, 813–823, https://doi.org/10.1038/ngeo1955, 2013.

Klappenbach, F., Bertleff, M., Kostinek, J., Hase, F., Blumenstock, T., Agusti-Panareda, A., Razinger, M., and Butz, A.: Accurate mobile remote sensing of XCO_2 and XCH_4 latitudinal transects from aboard a research vessel, Atmos. Meas. Tech., 8, 5023–5038, https://doi.org/10.5194/amt-8-5023-2015, 2015.

Knapp, M., Kleinschek, R., Hase, F., Agustí-Panareda, A., Inness, A., Barré, J., Landgraf, J., Borsdorff, T., Kinne, S., and Butz, A.: Shipborne measurements of XCO_2, XCH_4, and XCO above the Pacific Ocean and comparison to CAMS atmospheric analyses and S5P/TROPOMI, Earth Syst. Sci. Data, 13, 199–211, https://doi.org/10.5194/essd-13-199-2021, 2021.

Kobayashi, S., Ota, Y., Harada, Y., Ebita, A., Moriya, M., Onoda, H., Onogi, K., Kamahori, H., Kobayashi, C., Endo, H., Miyaoka, K., and Takahashi, K.: The JRA-55 Reanalysis: General Specifications and Basic Characteristics, J. Meteorol. Soc. Japan. Ser. II, 93, 5–48, https://doi.org/10.2151/jmsj.2015-001, 2015.

Kuze, A., Suto, H., Nakajima, M., and Hamazaki, T.: Thermal and near infrared sensor for carbon observation Fourier-transform spectrometer on the Greenhouse Gases Observing Satellite for greenhouse gases monitoring, Appl. Opt., 48, 6716, https://doi.org/10.1364/AO.48.006716, 2009.

Laughner, J. L., Roche, S., Kiel, M., Toon, G. C., Wunch, D., Baier, B. C., Biraud, S., Chen, H., Kivi, R., Laemmel, T., Mckain, K., Quéhé, P.-Y., Rousogenous, C., Stephens, B. B., Walker, K., and Wennberg, P. O.: A new algorithm to generate a priori trace gas profiles for the GGG2020 retrieval algorithm, Atmos. Meas. Tech., 1–41, 2022.

Lorente, A., Borsdorff, T., Butz, A., Hasekamp, O., Aan De Brugh, J., Schneider, A., Wu, L., Hase, F., Kivi, R., Wunch, D., Pollard, D. F., Shiomi, K., Deutscher, N. M., Velazco, V. A., Roehl, C. M., Wennberg, P. O., Warneke, T., and Landgraf, J.: Methane retrieved from TROPOMI: Improvement of the data product and validation of the first 2 years of measurements, Atmos. Meas. Tech., 14, 665–684, https://doi.org/10.5194/amt-14-665-2021, 2021.

Machida, T., Matsueda, H., Sawa, Y., Nakagawa, Y., Hirotani, K., Kondo, N., Goto, K., Nakazawa, T., Ishikawa, K., and Ogawa, T.: Worldwide Measurements of Atmospheric CO_2 and Other Trace Gas Species Using Commercial Airlines, J. Atmos. Ocean. Technol., 25, 1744–1754, https://doi.org/10.1175/2008JTECHA1082.1, 2008.

675 Matsueda, H., Machida, T., Sawa, Y., Nakagawa, Y., Hirotani, K., Ikeda, H., Kondo, N., and Goto, K.: Evaluation of atmospheric CO_2 measurements from new flask air sampling of JAL airliner observations, Pap. Meteorol. Geophys., 59, 1–17, https://doi.org/10.2467/mripapers.59.1, 2008.

Meirink, J. F., Eskes, H. J., and Goede, A. P. H.: Sensitivity analysis of methane emissions derived from SCIAMACHY observations through inverse modelling, Atmos. Chem. Phys., 6, 1275–1292, https://doi.org/10.5194/acp-6-1275-2006, 680 2006.

Morino, I., Ohyama, H., Hori, A., Ikegami, H.: TCCON data from Tsukuba (JP), 125HR, Release GGG2020.R0 (Version R0) [Data set]. CaltechDATA. https://doi.org/10.14291/tccon.ggg2020.tsukuba02.R0, 2022.

Müller, A., Tanimoto, H., Sugita, T., Machida, T., Nakaoka, S., Patra, P. K., Laughner, J., and Crisp, D.: New approach to evaluate satellite-derived XCO_2 over oceans by integrating ship and aircraft observations, Atmos. Chem. Phys., 21, 685 8255–8271, https://doi.org/10.5194/acp-21-8255-2021, 2021.

Myhre, G., Shindell, D., Bréon, F.-M., Collins, W., Fuglestvedt, J., Huang, J., Koch, D., Lamarque, J.-F., Lee, D., Mendoza, B., Nakajima, T., Robock, A., Stephens, G., Takemura, T., and Zhang, H.: Anthropogenic and Natural Radiative Forcing, in: Climate Change 2013 – The Physical Science Basis, edited by: Intergovernmental Panel on Climate Change, Cambridge University Press, Cambridge, 659–740, https://doi.org/10.1017/CBO9781107415324.018, 2013.

690 Nakajima, M., Kuze, A., Kawakami, S., Shiomi, K., and Suto, H.: Monitoring of the greenhouse gases from space by GOSAT, International Archives of the Photogrammetry, Remote Sensing and Spatial Information Sciences - ISPRS Archives, 38, 94–99, 2010.

Nara, H., Tanimoto, H., Tohjima, Y., Mukai, H., Nojiri, Y., and Machida, T.: Emissions of methane from offshore oil and gas platforms in Southeast Asia, Sci. Rep., 4, 1–6, https://doi.org/10.1038/srep06503, 2014.

695 NIES GOSAT Project: Release Note of Bias-corrected FTS SWIR Level 2 CO_2, CH_4 Products (V02.95/V02.96) for General Users", https://data2.gosat.nies.go.jp/doc/documents/ReleaseNote_FTSSWIRL2_BiasCorr_V02.95-V02.96_en.pdf, 2020, revised 2021, accessed on . [Verified 21 April 2023].

Nisbet, E. G., Manning, M. R., Dlugokencky, E. J., Fisher, R. E., Lowry, D., Michel, S. E., Myhre, C. L., Platt, S. M., Allen, G., Bousquet, P., Brownlow, R., Cain, M., France, J. L., Hermansen, O., Hossaini, R., Jones, A. E., Levin, I., Manning, 700 A. C., Myhre, G., Pyle, J. A., Vaughn, B. H., Warwick, N. J., and White, J. W. C.: Very Strong Atmospheric Methane Growth in the 4 Years 2014–2017: Implications for the Paris Agreement, Global Biogeochem. Cycles, 33, 318–342, https://doi.org/10.1029/2018GB006009, 2019.

Niwa, Y., Tsuboi, K., Matsueda, H., Sawa, Y., Machida, T., Nakamura, M., Kawasato, T., Saito, K., Takatsuji, S., Tsuji, K., Nishi, H., Dehara, K., Baba, Y., Kuboike, D., Iwatsubo, S., Ohmori, H., and Hanamiya, Y.: Seasonal variations of CO_2,

705   CH_4, N_2O and CO in the mid-troposphere over the western north pacific observed using a C-130H cargo aircraft, J. Meteorol. Soc. Japan, 92, 55–70, https://doi.org/10.2151/jmsj.2014-104, 2014.

Parker, R. J., Boesch, H., Wooster, M. J., Moore, D. P., Webb, A. J., Gaveau, D., and Murdiyarso, D.: Atmospheric CH_4 and CO_2 enhancements and biomass burning emission ratios derived from satellite observations of the 2015 Indonesian fire plumes, Atmos. Chem. Phys., 16, 10111–10131, https://doi.org/10.5194/acp-16-10111-2016, 2016.

710   Patra, P. K., Takigawa, M., Ishijima, K., Choi, B. C., Cunnold, D., Dlugokencky, E. J., Fraser, P., Gomez-Pelaez, A. J., Goo, T. Y., Kim, J. S., Krummel, P., Langenfelds, R., Meinhardt, F., Mukai, H., O'Doherty, S., Prinn, R. G., Simmonds, P., Steele, P., Tohjima, Y., Tsuboi, K., Uhse, K., Weiss, R., Worthy, D., and Nakazawa, T.: Growth rate, seasonal, synoptic, diurnal variations and budget of methane in the lower atmosphere, Journal of the Meteorological Society of Japan, 87, 635–663, https://doi.org/10.2151/jmsj.87.635, 2009.

715   Patra, P. K., Saeki, T., Dlugokencky, E. J., Ishijima, K., Umezawa, T., Ito, A., Aoki, S., Morimoto, S., Kort, E. A., Crotwell, A., Ravi Kumar, K., and Nakazawa, T.: Regional methane emission estimation based on observed atmospheric concentrations (2002-2012), J. Meteorol. Soc. Japan, 94, 91–113, https://doi.org/10.2151/jmsj.2016-006, 2016.

Patra, P. K., Takigawa, M., Watanabe, S., Chandra, N., Ishijima, K., and Yamashita, Y.: Improved Chemical Tracer Simulation by MIROC4.0-based Atmospheric Chemistry-Transport Model (MIROC4-ACTM), SOLA, 14, 91–96,
720   https://doi.org/10.2151/sola.2018-016, 2018.

Peng, S., Lin, X., Thompson, R. L., Xi, Y., Liu, G., Hauglustaine, D., Lan, X., Poulter, B., Ramonet, M., Saunois, M., Yin, Y., Zhang, Z., Zheng, B., and Ciais, P.: Wetland emission and atmospheric sink changes explain methane growth in 2020, Nature, 612, 477–482, https://doi.org/10.1038/s41586-022-05447-w, 2022.

Rodgers, C. D.: Inverse Methods for Atmospheric Sounding, WORLD SCIENTIFIC, https://doi.org/10.1142/3171, 2000.

725   Saito, K.: Atmospheric CH_4 by Aircraft (Western North Pacific), Japan Meteorological Agency, dataset published as CH4_AOA_aircraft-flask_JMA_data1 at WDCGG, ver.2022-02-15-0845, https://doi.org/10.50849/WDCGG_0001-8002-1002-05-02-9999, accessed on 5 December 2022.

Saunois, M., Stavert, A., Poulter, B., Bousquet, P., Canadell, J., Jackson, R., Raymond, P., Dlugokencky, E., Houweling, S., Patra, P., Ciais, P., Arora, V., Bastviken, D., Bergamaschi, P., Blake, D., Brailsford, G., Bruhwiler, L., Carlson, K.,
730   Carrol, M., Castaldi, S., Chandra, N., Crevoisier, C., Crill, P., Covey, K., Curry, C., Etiope, G., Frankenberg, C., Gedney, N., Hegglin, M., Höglund-Isaksson, L., Hugelius, G., Ishizawa, M., Ito, A., Janssens-Maenhout, G., Jensen, K., Joos, F., Kleinen, T., Krummel, P., Langenfelds, R., Laruelle, G., Liu, L., Machida, T., Maksyutov, S., McDonald, K., McNorton, J., Miller, P., Melton, J., Morino, I., Müller, J., Murguia-Flores, F., Naik, V., Niwa, Y., Noce, S., O'Doherty, S., Parker, R., Peng, C., Peng, S., Peters, G., Prigent, C., Prinn, R., Ramonet, M., Regnier, P., Riley, W., Rosentreter, J.,
735   Segers, A., Simpson, I., Shi, H., Smith, S., Steele, L. P., Thornton, B., Tian, H., Tohjima, Y., Tubiello, F., Tsuruta, A., Viovy, N., Voulgarakis, A., Weber, T., van Weele, M., van der Werf, G., Weiss, R., Worthy, D., Wunch, D., Yin, Y., Yoshida, Y., Zhang, W., Zhang, Z., Zhao, Y., Zheng, B., Zhu, Q., Zhu, Q., and Zhuang, Q.: The Global Methane Budget 2000–2017, Earth Syst. Sci. Data, 12, 1561–1623, https://doi.org/10.5194/essd-12-1561-2020, 2020.

Schneising, O., Buchwitz, M., Reuter, M., Heymann, J., Bovensmann, H., and Burrows, J. P.: Long-term analysis of carbon dioxide and methane column-averaged mole fractions retrieved from SCIAMACHY, Atmos. Chem. Phys., 11, 2863–2880, https://doi.org/10.5194/acp-11-2863-2011, 2011.

Segers, A. and Steinke, T.: Evaluation and quality-control document for observation-based CH_4 flux estimates for the period 1990-2020, 1–44, 2022.

Shindell, D., Kuylenstierna, J. C. I., Vignati, E., van Dingenen, R., Amann, M., Klimont, Z., Anenberg, S. C., Muller, N., Janssens-Maenhout, G., Raes, F., Schwartz, J., Faluvegi, G., Pozzoli, L., Kupiainen, K., Höglund-Isaksson, L., Emberson, L., Streets, D., Ramanathan, V., Hicks, K., Oanh, N. T. K., Milly, G., Williams, M., Demkine, V., and Fowler, D.: Simultaneously Mitigating Near-Term Climate Change and Improving Human Health and Food Security, Science (80-.)., 335, 183–189, https://doi.org/10.1126/science.1210026, 2012.

Shiomi, K., Kawakami, S., Ohyama, H., Arai, K., Okumura, H., Ikegami, H., Usami, M.: TCCON data from Saga (JP), Release GGG2020.R0 (Version R0) [Data set]. CaltechDATA. https://doi.org/10.14291/tccon.ggg2020.saga01.R0, 2022.

Stevenson, D. S., Derwent, R. G., Wild, O., and Collins, W. J.: COVID-19 lockdown emission reductions have the potential to explain over half of the coincident increase in global atmospheric methane, Atmos. Chem. Phys., 22, 14243–14252, https://doi.org/10.5194/acp-22-14243-2022, 2022.

Suto, H., Kataoka, F., Kikuchi, N., Knuteson, R. O., Butz, A., Haun, M., Buijs, H., Shiomi, K., Imai, H., and Kuze, A.: Thermal and near-infrared sensor for carbon observation Fourier transform spectrometer-2 (TANSO-FTS-2) on the Greenhouse gases Observing SATellite-2 (GOSAT-2) during its first year in orbit, Atmos. Meas. Tech., 14, 2013–2039, https://doi.org/10.5194/amt-14-2013-2021, 2021.

Szopa, S., Naik, V., Adhikary, B., Artaxo, P., Berntsen, T., Collins, W. D., Fuzzi, S., Gallardo, L., Kiendler Scharr, A., Klimont, Z., Liao, H., Unger, N., and Zanis, P.: Short-Lived Climate Forcers. In: Climate Change 2021: The Physical Science Basis. Contribution of Working Group I to the Sixth Assessment Report of the Intergovernmental Panel on Climate Change, 817–922 pp., https://doi.org/10.1017/9781009157896.008, 2021.

Takagi, H., Houweling, S., Andres, R. J., Belikov, D., Bril, A., Boesch, H., Butz, A., Guerlet, S., Hasekamp, O., Maksyutov, S., Morino, I., Oda, T., O'Dell, C. W., Oshchepkov, S., Parker, R., Saito, M., Uchino, O., Yokota, T., Yoshida, Y., and Valsala, V.: Influence of differences in current GOSAT X CO_2 retrievals on surface flux estimation, Geophys. Res. Lett., 41, 2598–2605, https://doi.org/10.1002/2013GL059174, 2014.

Terao, Y., Mukai, H., Nojiri, Y., MacHida, T., Tohjima, Y., Saeki, T., and Maksyutov, S.: Interannual variability and trends in atmospheric methane over the western Pacific from 1994 to 2010, J. Geophys. Res. Atmos., 116, https://doi.org/10.1029/2010JD015467, 2011.

Tohjima, Y., Machida, T., Utiyama, M., Katsumoto, M., Fujinuma, Y., and Maksyutov, S.: Analysis and presentation of in situ atmospheric methane measurements from Cape Ochi-ishi and Hateruma Island, J. Geophys. Res. Atmos., 107, 1–11, https://doi.org/10.1029/2001jd001003, 2002.

Travis, K. R., Heald, C. L., Allen, H. M., Apel, E. C., Arnold, S. R., Blake, D. R., Brune, W. H., Chen, X., Commane, R., Crounse, J. D., Daube, B. C., Diskin, G. S., Elkins, J. W., Evans, M. J., Hall, S. R., Hintsa, E. J., Hornbrook, R. S.,

775   Kasibhatla, P. S., Kim, M. J., Luo, G., McKain, K., Millet, D. B., Moore, F. L., Peischl, J., Ryerson, T. B., Sherwen, T., Thames, A. B., Ullmann, K., Wang, X., Wennberg, P. O., Wolfe, G. M., and Yu, F.: Constraining remote oxidation capacity with ATom observations, Atmos. Chem. Phys., 20, 7753–7781, https://doi.org/10.5194/acp-20-7753-2020, 2020.

Tsuboi, K., Matsueda, H., Sawa, Y., Niwa, Y., Nakamura, M., Kuboike, D., Saito, K., Ohmori, H., Iwatsubo, S., Nishi, H.,

780   Hanamiya, Y., Tsuji, K., and Baba, Y.: Evaluation of a new JMA aircraft flask sampling system and laboratory trace gas analysis system, Atmos. Meas. Tech., 6, 1257–1270, https://doi.org/10.5194/amt-6-1257-2013, 2013.

Umezawa, T., Machida, T., Ishijima, K., Matsueda, H., Sawa, Y., Patra, P. K., Aoki, S., and Nakazawa, T.: Carbon and hydrogen isotopic ratios of atmospheric methane in the upper troposphere over the Western Pacific, Atmos. Chem. Phys., 12, 8095–8113, https://doi.org/10.5194/acp-12-8095-2012, 2012.

785 Umezawa, T., Goto, D., Aoki, S., Ishijima, K., Patra, P. K., Sugawara, S., Morimoto, S., and Nakazawa, T.: Variations of tropospheric methane over Japan during 1988-2010, Tellus, Ser. B Chem. Phys. Meteorol., 66, https://doi.org/10.3402/tellusb.v66.23837, 2014.

Veefkind, J. P., Aben, I., McMullan, K., Förster, H., de Vries, J., Otter, G., Claas, J., Eskes, H. J., de Haan, J. F., Kleipool, Q., van Weele, M., Hasekamp, O., Hoogeveen, R., Landgraf, J., Snel, R., Tol, P., Ingmann, P., Voors, R., Kruizinga, B.,

790   Vink, R., Visser, H., and Levelt, P. F.: TROPOMI on the ESA Sentinel-5 Precursor: A GMES mission for global observations of the atmospheric composition for climate, air quality and ozone layer applications, Remote Sens. Environ., 120, 70–83, https://doi.org/10.1016/j.rse.2011.09.027, 2012.

Whitburn, S., Van Damme, M., Clarisse, L., Turquety, S., Clerbaux, C., and Coheur, P.-F.: Doubling of annual ammonia emissions from the peat fires in Indonesia during the 2015 El Niño, Geophys. Res. Lett., 43, 11,007-11,014,

795   https://doi.org/10.1002/2016GL070620, 2016.

Wilcox, L. J., Hoskins, B. J., and Shine, K. P.: A global blended tropopause based on ERA data. Part I: Climatology, Q. J. R. Meteorol. Soc., 138, 561–575, https://doi.org/10.1002/qj.951, 2012.

Wofsy, S. C.: HIAPER Pole-to-Pole Observations (HIPPO): fine-grained, global-scale measurements of climatically important atmospheric gases and aerosols, Philos. Trans. R. Soc. A Math. Phys. Eng. Sci., 369, 2073–2086,

800   https://doi.org/10.1098/rsta.2010.0313, 2011.

Wunch, D., Toon, G. C., Blavier, J.-F. L., Washenfelder, R. A., Notholt, J., Connor, B. J., Griffith, D. W. T., Sherlock, V., and Wennberg, P. O.: The Total Carbon Column Observing Network, Philos. Trans. R. Soc. A Math. Phys. Eng. Sci., 369, 2087–2112, https://doi.org/10.1098/rsta.2010.0240, 2011.

Yoshida, Y., Ota, Y., Eguchi, N., Kikuchi, N., Nobuta, K., Tran, H., Morino, I., and Yokota, T.: Retrieval algorithm for CO_2

805   and CH_4 column abundances from short-wavelength infrared spectral observations by the Greenhouse gases observing satellite, Atmos. Meas. Tech., 4, 717–734, https://doi.org/10.5194/amt-4-717-2011, 2011.

Yoshida, Y., Kikuchi, N., Morino, I., Uchino, O., Oshchepkov, S., Bril, A., Saeki, T., Schutgens, N., Toon, G. C., Wunch, D., Roehl, C. M., Wennberg, P. O., Griffith, D. W. T., Deutscher, N. M., Warneke, T., Notholt, J., Robinson, J., Sherlock, V., Connor, B., Rettinger, M., Sussmann, R., Ahonen, P., Heikkinen, P., Kyrö, E., Mendonca, J., Strong, K., Hase, F., Dohe, S., and Yokota, T.: Improvement of the retrieval algorithm for GOSAT SWIR XCO$_2$ and XCH$_4$ and their validation using TCCON data, Atmos. Meas. Tech., 6, 1533–1547, https://doi.org/10.5194/amt-6-1533-2013, 2013.

Yoshida, Y., Someya, Y., Ohyama, H., Morino, I., Matsunaga, T., Deutscher, N. M., Griffith, D. W. T., Hase, F., Iraci, L. T., Kivi, R., Notholt, J., Pollard, D. F., Té, Y., Velazco, V. A., Wunch, D.: Quality evaluation of the column-averaged dry air mole fractions of carbon dioxide and methane observed by GOSAT and GOSAT-2, Scientific Online Letters on the Atmosphere (SOLA), 19, 173–184, https://doi.org/10.2151/sola.2023-023, ~~in press,~~ 2023.

Zhang, Z., Zimmermann, N. E., Calle, L., Hurtt, G., Chatterjee, A., and Poulter, B.: Enhanced response of global wetland methane emissions to the 2015–2016 El Niño-Southern Oscillation event, Environ. Res. Lett., 13, 074009, https://doi.org/10.1088/1748-9326/aac939, 2018.

Zhang, Z., Poulter, B., Knox, S., Stavert, A., McNicol, G., Fluet-Chouinard, E., Feinberg, A., Zhao, Y., Bousquet, P., Canadell, J. G., Ganesan, A., Hugelius, G., Hurtt, G., Jackson, R. B., Patra, P. K., Saunois, M., Höglund-Isaksson, L., Huang, C., Chatterjee, A., and Li, X.: Anthropogenic emission is the main contributor to the rise of atmospheric methane during 1993–2017, Natl. Sci. Rev., 9, https://doi.org/10.1093/nsr/nwab200, 2022.

Zhao, Y., Saunois, M., Bousquet, P., Lin, X., Berchet, A., Hegglin, M. I., Canadell, J. G., Jackson, R. B., Hauglustaine, D. A., Szopa, S., Stavert, A. R., Luke Abraham, N., Archibald, A. T., Bekki, S., Deushi, M., Jöckel, P., Josse, B., Kinnison, D., Kirner, O., Marécal, V., O'Connor, F. M., Plummer, D. A., Revell, L. E., Rozanov, E., Stenke, A., Strode, S., Tilmes, S., Dlugokencky, E. J., and Zheng, B.: Inter-model comparison of global hydroxyl radical (OH) distributions and their impact on atmospheric methane over the 2000-2016 period, Atmos. Chem. Phys., 19, 13701–13723, https://doi.org/10.5194/acp-19-13701-2019, 2019.